Electronic ISSN: 1309-0267

International Journal of Engineering & Applied Sciences

IJEAS

I J E A S

Volume 11, Issue 2
2019

Published by Akdeniz University

Editorial Board

(The name listed below is not Alphabetical or any title scale)

Abstracting & Indexing

IJEAS provides unique **DOI** link to every paper published.

Editorial Scope

The journal presents its readers with broad coverage across some branches of engineering and science of the latest development and application of new solution algorithms, artificial intelligent techniques innovative numerical methods and/or solution techniques directed at the utilization of computational methods in solid and nano-scaled mechanics.

International Journal of Engineering & Applied Sciences (IJEAS) is an Open Access Journal

International Journal of Engineering & Applied Sciences (IJEAS) publish original contributions on the following topics:

Numerical Methods in Solid Mechanics

Nanomechanic and applications

Microelectromechanical systems (MEMS)

Vibration Problems in Engineering

Higher order elasticity (Strain gradient, couple stress, surface elasticity, nonlocal elasticity)

Applied Mathematics

CONTENTS

International Journal of Engineering & Applied Sciences (IJEAS)
Vol.11, Issue 2 (2019) 369-386
http://dx.doi.org/10.24107/ijeas.567435
Int J Eng Appl Sci 11(2) (2019) 369-386

Vibro-Electrical Behavior of a Viscoelastic Piezo-Nanowire in an Elastic Substrate Considering Stress Nonlocality and Microstructural Size-Dependent Effects

Mohammad Malikan

Department of Mechanical Engineering, Faculty of Engineering, Islamic Azad University, Mashhad Branch, Mashhad, Iran

E-mail address: mohammad.malikan@yahoo.com

ORCID numbers of authors:
0000-0001-7356-2168

Received date: 18.05.2019
Accepted date: 25.06.2019

Abstract

This research deals with dynamic response of a Polymer/$BaTiO_3$ nanowire including viscosity influences. The wire is also impressed by a longitudinal electric field. Hamilton's principle, Lagrangian strains and a refined higher-order beam theory are combined together in order to derive equations of motion. By combining nonlocality and small size effects of a unique model into the derived equations, the couple relations which describe nanosize behavior in a small scale are presented. By employing an analytical approach, the fundamental natural frequencies are calculated numerically. The important results display that the effect of internal viscosity and nonlocality whenever the nanowire is very large are pointless.

Keywords: Dynamics response; Piezo-nanowires; Viscosity; Nonlocal theory of strain gradient; Analytical approach

1. Introduction and Literature review

In continuation of discovering of carbon nanotubes by Ijimia in 1991, a wide attention has been paid to the other one-dimensional nanomaterials for example; nanobelts, nanorods and nanowires [1]. Quasi aforementioned one-dimensional materials are a new group which in recent years have been presented in many scientific research. It was proved that these materials with a non-carbonic base show the amazing optic, thermal and mechanical characteristics and are utilized as main structural group in nanoscience and nanotechnology for equipment such as biological and chemical sensors, field effect transistors and logic circuits [2].

Paying attention to the new shape of nanostructures, namely nanowires, has been doubled after year 2000. The structures with thickness or diameter of a few tens of nanometers and even smaller and also non-limited length can be defined as nanowires. The nanowires' cross section might be cylindrical, hexagonal, polygons or etc. with regard to their crystallography [3]. The nanowires' length can be variable from a few tens of nanometers to micron or even millimeter. These nanostructures regarding their special properties can be used in the new

electronic parts. Because developments and progressives in the electronic industries are due to the decreasing of their parts [4].

One of the most attractive nanostructures can be nanowires made of metals due to their unique properties, which lead to their various applications. Nanowires can be used on computers and other calculating devices. Nanoscale wires are required to achieve complex nanoscale electronics. In addition, the nanowires itself can be the basis of electronic components, such as memory [4]. Proper understanding of the properties, applications, and methods of making nanowires is very important because it will enable researchers to construct nanowires with controlled properties and dimensions and can easily adapt them to fit the structural elements in minimizing electrical and electronic equipment [3].

Theoretical investigations on the prediction of mechanical response of nanowires are rare and there have been a few studies about nanowires. Kiani [5] analyzed dynamically a nanowire exposed to a longitudinal magnetic shock. He assumed wires on an elastic foundation and used nonlocal continuum theory to study quantum effects. He also solved the obtained equations of motion by a semi-analytical approach. In another study, Kiani [6] examined a double current-carrying nanowire exposed to a longitudinal magnetic field based on a new integro-surface energy method. Pishkenari et al. [7] studied transverse natural frequencies of a silicon nanowire using atomistic simulation method. To model the nanoscale, they proposed a new continuum model at which surface stress and surface elasticity were considered by both Timoshenko and Euler-Bernoulli beam models. Their outcomes estimated the results for Timoshenko approach including surface effects are matched with MD results. Fu and Zhang [8] reported stability critical conditions and free torsional natural frequencies of an established continuum core-shell nanowire which included weak interfaces based on the surface elasticity. Dynamic buckling and free vibrations of a nanowire with an initial deformation considering surface effects were investigated by Kiani [9]. The nanowire was placed in an axial magnetic surround and frequencies of vibration were computed analytically. Gongbai et al. [10] investigated harmonic and transient response of an atomic nanowire made of silicon. Zhoua et al. [11] formulated nonlinear resonance of a ZnO piezo-nanowire derived by an electric field. Their results agreed with the experimental outcomes. Zhang et al. [12] combined the Euler-Bernoulli approach and a high-order surface stress in order to study transverse vibrations of a nanowire placed in a polymer foundation exposed to an axial compressive force. The pivot boundary condition was satisfied analytically based on a closed-form solution. Li et al. [13] demonstrated three different elastic substrates for analysis free natural and excitation frequencies of a nanowire. The governing equations were derived regarding a surface elasticity and solved respecting to various boundary conditions. Su et al. [14] addressed small scale effects for considering mechanically transverse response of several nanostructures with one-dimension like nanoropes and nanowires. They presented the strain gradient model to examine small size influences and obtained constitutive equations on the basis of classical beam theory. Finally they computed free vibrations and buckling of the models under several edge conditions and validated the numerical results with the experimental tests. Samaei et al. [15] presented free vibration of a piezo-nanowire under an electric field for which surface effects addressed size influences. The simply-supported rectangular wire was modeled analytically on the basis of both Timoshenko and Euler-Bernoulli beam approaches. Their outcomes showed that the shear deformations imposed a remarkable impact on the dynamics characteristics of the nanowire. Gheshlaghi and Hasheminejad [16] analyzed dynamically a piezo-nanowire included both nonlocal and surface elasticity effects based on the classic beam theory. An explicit solution technique was devoted to compute natural frequencies of the wire. Kiani also published some other research works related to the nanowires [17-19]. Mercan et al. [20] modeled stability of a Silicon

Carbide nanowire on the basis of a higher-order elasticity theory. Mercan and Civalek [21] analyzed dynamically a micro/nanowire based on the finite element model. On the other hand, Numanoglu et al. [22] examined natural frequencies of an Au nanowire based on the continuum elasticity approach. In terms of nanostructures analyses, there are a wide range of valuable published research in several conditions [23-65].

Heretofore by review the literature, it is clear that the nanowires have been examined rarely which the most important ones are above mentioned. However within the published research there is no one in which a nanowire has viscoelastic influences. There is no doubt that considering a viscoelastic piezo-nanowire can lead to attractive results. Additionally, the Polymer/$BaTiO_3$ nanowire has been rarely investigated. Therefore, in this paper it is tried to show a new schema for analysis of nanowires. To this, a modified beam model is employed from which one equation is obtained only whenever the classical mechanics is taken into consideration. To be the small scale influences taken into account, nonlocal strain gradient theory is applied. This model examines both size-dependent and nonlocality characteristics. In order to simply transfer the partial differential equation into the algebraic one the Navier method is utilized. This method fully satisfies pivot boundary condition. Afterwards, the outcomes for variety of cases would be depicted numerically.

2. Theoretical Modelling

A $BaTiO_3$ nanowire is lied in a polymer matrix and displayed by Figure below. Cartesian coordinate is connected to the center of the wire (x) and along the upper quadrant of its diameter (z).

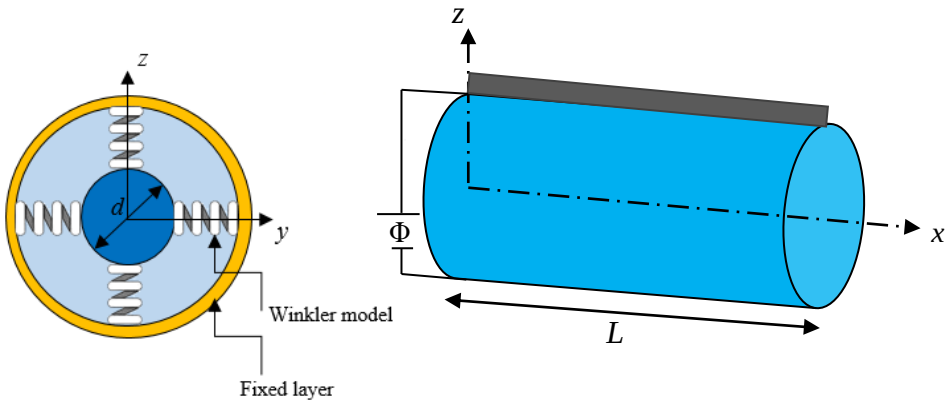

Fig. 1. A Polymer/$BaTiO_3$ nanowire in a Cartesian coordinate system

Regarding the refined shear deformation beam theory [48], the given displacement field is described as

$$\begin{Bmatrix} U(x,z,t) \\ W(x,z,t) \end{Bmatrix} = \begin{Bmatrix} u_0(x,t) - z\dfrac{\partial w_0(x,t)}{\partial x} \\ w_0(x,t) + B\dfrac{\partial^2 w_0(x,t)}{\partial x^2} \end{Bmatrix} \tag{1}$$

In which B becomes $B = \dfrac{D_{11}}{A_{44}}$.

The dynamic equilibrium of the model is derived with the calculus of variations on the basis of the Hamilton's principle leading to formulating governing equations [48]

$$\delta\Pi = \int_0^t \left(\delta\Omega - \delta S + \delta T\right)dt = 0 \tag{2}$$

where Π depicts total potential energy of the wire, T and Ω denote the kinetic energy and the work done by outer loads. S also symbolizes the strain energy of the wire.

2.1. The strain potential energy

The strain energy would be shown in a variational form as [48]

$$\delta S = \iiint_v \left(\sigma_{ij}\delta\varepsilon_{ij} - D_i\delta E_i\right)dV = 0 \tag{3}$$

In which the aforementioned parameters are respectively the electric field (E_i), electric displacement (D_i), strain tensor (ε_{ij}), and stress tensor (σ_{ij}), and can be summarized as follows [49]

$$\sigma_{ij} = C_{ijkl}\varepsilon_{kl} - e_{ijk}E_k \tag{4}$$

$$D_i = e_{ikl}\varepsilon_{kl} + \kappa_{ik}E_k \tag{5}$$

where the displayed constants are piezoelectric (e_{ijk}), dielectric (κ_{ik}), and elasticity quantities (C_{ijkl}). The tensors in Eqs. (4-5) lead to [49]:

$$e_{ijk} = \begin{Bmatrix} \bar{e}_{31} \\ \bar{e}_{15} \end{Bmatrix} \tag{6}$$

$$\kappa_{ik} = \begin{Bmatrix} \bar{\kappa}_{11} \\ \bar{\kappa}_{33} \end{Bmatrix} \tag{7}$$

$$\begin{Bmatrix} \bar{e}_{31} \\ \bar{e}_{15} \\ \bar{\kappa}_{11} \\ \bar{\kappa}_{33} \end{Bmatrix} = \begin{Bmatrix} e_{31} - \dfrac{C_{13}e_{33}}{C_{33}} \\ e_{15} \\ \kappa_{11} \\ \kappa_{33} + \dfrac{e_{33}^2}{C_{33}} \end{Bmatrix} \tag{8a-d}$$

$$\varepsilon_{ij} = \frac{1}{2}\left(\frac{\partial u_i}{\partial x_j} + \frac{\partial u_j}{\partial x_i} + \frac{\partial u_k}{\partial x_i}\frac{\partial u_k}{\partial x_j}\right) \Rightarrow$$

$$\begin{Bmatrix} \varepsilon_{xx} \\ \gamma_{xz} \end{Bmatrix} = \begin{Bmatrix} \dfrac{\partial u_0}{\partial x} - z\dfrac{\partial^2 w_0}{\partial x^2} + \dfrac{1}{2}\left(B\dfrac{\partial^3 w_0}{\partial x^3} + \dfrac{\partial w_0}{\partial x}\right)^2 \\ B\dfrac{\partial^3 w_0}{\partial x^3} \end{Bmatrix} \tag{9a-b}$$

A potential function for the longitudinal electric field can be chosen as [49].

$$\overline{\Phi}\ (x,z,t)=-\cos\left(\frac{\pi z}{d}\right)\Phi\ (x,t)+\frac{2zV_0}{d}e^{i\omega t} \tag{10}$$

In which $\Phi\ (x,t)$ denotes the electric field and the outer electric voltage is shown by V_0. Afterwards, the piezoelectric components take the form [49]:

$$E_i=\begin{Bmatrix}\overline{E}_x\\ \overline{E}_z\end{Bmatrix}=\begin{Bmatrix}-\dfrac{\partial\overline{\Phi}(x,t)}{\partial x}\\ -\dfrac{\partial\overline{\Phi}(x,t)}{\partial z}\end{Bmatrix}=\begin{Bmatrix}\cos\left(\dfrac{\pi z}{d}\right)\dfrac{\partial\Phi(x,t)}{\partial x}\\ -\dfrac{\pi}{d}\sin\left(\dfrac{\pi z}{d}\right)\Phi(x,t)-\dfrac{2V_0}{d}e^{i\omega t}\end{Bmatrix} \tag{11a-b}$$

The electric displacements can be expressed as [49]:

$$D_i=\begin{Bmatrix}\overline{D}_x\\ \overline{D}_z\end{Bmatrix}=\begin{Bmatrix}\int_{-d/2}^{d/2}D_x\cos\left(\dfrac{\pi z}{d}\right)dz\\ \int_{-d/2}^{d/2}\dfrac{\pi}{d}D_z\cos\left(\dfrac{\pi z}{d}\right)dz\end{Bmatrix}=\begin{Bmatrix}E_{15}B\dfrac{\partial^3 w_0}{\partial x^3}+X_{11}\dfrac{\partial\Phi}{\partial x}\\ -E_{31}\dfrac{\partial^2 w_0}{\partial x^2}-X_{33}\Phi\end{Bmatrix} \tag{12a-b}$$

The coefficients in Eq. (12) are developed as

$$\begin{Bmatrix}E_{31}\\ E_{15}\\ X_{11}\\ X_{33}\end{Bmatrix}=\int_{-d/2}^{d/2}\begin{Bmatrix}\bar{e}_{31}\dfrac{\pi}{d}z\sin\left(\dfrac{\pi}{d}z\right)\\ \bar{e}_{15}\cos\left(\dfrac{\pi}{d}z\right)\\ \bar{\kappa}_{11}\cos^2\left(\dfrac{\pi}{d}z\right)\\ \bar{\kappa}_{33}\left(\dfrac{\pi}{d}\right)^2\sin^2\left(\dfrac{\pi}{d}z\right)\end{Bmatrix}dz \tag{13a-d}$$

2.2. The external force

The Winkler model as an external force makes a thermodynamic work calculated as [48-49]

$$\delta\Omega=-\int\int_A k_w\frac{\partial^2 w_0}{\partial x^2}\delta w_0\,dx=0 \tag{14}$$

where k_w demonstrates the value of springiness in the foundation.

2.3. The kinetic energy

The kinetic energy is written as [48]

$$T=\frac{1}{2}\rho\int\int_A\left(\left(\frac{\partial U}{\partial t}\right)^2+\left(\frac{\partial W}{\partial t}\right)^2\right)dA\,dz=0 \tag{15}$$

Applying the variational form of the kinetic energy, one gets

$$\begin{aligned}\delta T = \rho\int \int_A \left(-\frac{\partial^2 u_0}{\partial t^2}+z\,\frac{\partial^3 w_0}{\partial x\,\partial t^2}\right)\delta u_0+\left(z\,\frac{\partial^3 u_0}{\partial x\,\partial t^2}-z^2\left(\frac{\partial^2 w_0}{\partial x\,\partial t}\right)^2\right.\\ \left.-z^2\,\frac{\partial^4 w_0}{\partial x^2\partial t^2}-\frac{\partial^2 w_0}{\partial t^2}-B^2\,\frac{\partial^6 w_0}{\partial x^4\partial t^2}-2B\,\frac{\partial^4 w_0}{\partial x^2\partial t^2}\right)\delta w_0 dA\,dz=0\end{aligned} \tag{16}$$

where $I_m\left(I_m=\rho I_c\right)$ shows the mass moment of inertia, m_0 $\left(m_0=\rho\int_A dA\right)$ is the volumetric mass density, and ρ exhibits the sectional density.

Finally, doing $\delta\Pi=0$ gives problem equations as

$$\delta u_0:\frac{\partial N_x}{\partial x}=0 \tag{17a}$$

$$\begin{aligned}\delta w_0:-\frac{\partial^2 M_x}{\partial x^2}+B\,\frac{\partial^3 Q_x}{\partial x^3}+N_x\left(B^2\,\frac{\partial^6 w_0}{\partial x^6}+2B\,\frac{\partial^4 w_0}{\partial x^4}+\frac{\partial^2 w_0}{\partial x^2}\right)-k_w\,\frac{\partial^2 w_0}{\partial x^2}\\ -I_m\left(\frac{\partial^4 w_0}{\partial x^2\partial t^2}\right)-m_0\times\left(\frac{\partial^2 w_0}{\partial t^2}+B^2\,\frac{\partial^6 w_0}{\partial x^4\partial t^2}+2B\,\frac{\partial^4 w_0}{\partial x^2\partial t^2}\right)=0\end{aligned} \tag{17b}$$

$$\delta\Phi=0:\int_{-d/2}^{d/2}\left[\frac{\partial\overline{D}_x}{\partial x}cos\left(\frac{\pi z}{d}\right)+\frac{\pi}{d}\overline{D}_z\,sin\left(\frac{\pi z}{d}\right)\right]dz=0 \tag{17c}$$

In which N_x, M_x and Q_x symbolize respectively the in-plane, moment and shear stress resultants.
The stress resultants are written as

$$\begin{Bmatrix}M_x\\Q_x\end{Bmatrix}=\int_A\begin{Bmatrix}\sigma_x z\\\sigma_{xz}\end{Bmatrix}dA \tag{18a-b}$$

Therefore Eq. (18) is rewritten as

$$\begin{Bmatrix}M_x\\Q_x\end{Bmatrix}=\begin{Bmatrix}-D_{11}\,\frac{\partial^2 w_0}{\partial x^2}\\A_{44}\left(B\,\frac{\partial^3 w_0}{\partial x^3}\right)\end{Bmatrix}+\begin{Bmatrix}E_{31}\Phi\\-E_{15}\,\frac{\partial\Phi}{\partial x}\end{Bmatrix} \tag{19a-b}$$

where the coefficients are

$$A_{44}=A\overline{C}_{44}\ ,\ D_{11}=\overline{C}_{11}I_c \tag{20a-b}$$

$$\begin{Bmatrix}\overline{C}_{11}\\\overline{C}_{44}\end{Bmatrix}=\begin{Bmatrix}C_{11}-\frac{C_{13}^2}{C_{33}}\\C_{44}\end{Bmatrix} \tag{21a-b}$$

A reveals the nanowire' cross section. Furthermore, I_c $\left(I_c = \frac{\pi d^4}{64}\right)$ represents the area moment of the cross section.

In this research, axial stress resultant addresses the longitudinal electric load (N_{ij}^{E}) created by the electric field as [49]:

$$N_x^E = \int_{-d/2}^{d/2} \bar{e}_{31} \frac{2V_0}{d} dz \tag{22}$$

The equation below is applied to address the nonlocal strain gradient theory (NSGT) [66]. Efficiency and accuracy of NSGT as a size-dependent model was approved in many papers and this nanoscale approach is now a well-known one. Therefore, in this research the NSGT is used corresponding to

$$\begin{aligned} &\left(1-\mu\nabla^2\right)\sigma_{ij} = C_{ijkl}\left(1-l^2\nabla^2\right)\varepsilon_{kl} \ ; \\ &\left\langle \mu(nm^2) = \left(e_0 a\right)^2,\ \nabla^2 = \frac{\partial^2}{\partial x^2} \right\rangle \end{aligned} \tag{23}$$

In which μ depicts nonlocality and also l symbloizes a length scale factor for NSGT.

With regard to the Eq. (23) and applying it on the Eq. (19) the small scale stress resultants can be given by

$$\left(1-\mu\nabla^2\right)M_x = -\left(1-l^2\nabla^2\right)\left(D_{11}\frac{\partial^2 w_0}{\partial x^2}\right) + E_{31}\Phi \tag{24a}$$

$$\left(1-\mu\nabla^2\right)Q_x = \left(1-l^2\nabla^2\right)A_{44}\left(B\frac{\partial^3 w_0}{\partial x^3}\right) - E_{15}\frac{\partial\Phi}{\partial x} \tag{24b}$$

The linear model of viscoelasticity, namely Kelvin-Voigt is here utilized to consider coupling of Viscous-Elasticity in the nanowire as [67]

$$\sigma(t) = E(t)\varepsilon(t) = E\left(1+g\frac{\partial}{\partial t}\right)\varepsilon(t) \tag{25}$$

In which the viscoelastic factor is represented by g. Now the equations below are achieved which include a combination of Eq. (17) with Eqs. (12), (22), (24) and (25). The obtained relations should be utilized in order to compute the vibration frequencies of the piezo-nanowire with viscoelasticity properties.

$$\left(1-l^2\nabla^2\right)\left[\left(1+g\frac{\partial}{\partial t}\right)\left(D_{11}\frac{\partial^4 w_0}{\partial x^4}+A_{44}B^2\frac{\partial^6 w_0}{\partial x^6}\right)-\left(BE_{15}+E_{31}\right)\frac{\partial^2\Phi}{\partial x^2}-\right.$$
$$\left(1-\mu\nabla^2\right)N_x^E\left(B^2\frac{\partial^6 w_0}{\partial x^6}+2B\frac{\partial^4 w_0}{\partial x^4}+\frac{\partial^2 w_0}{\partial x^2}\right)+\left(1-\mu\nabla^2\right)\times$$
$$\left.\left[-I_m\left(\frac{\partial^4 w_0}{\partial x^2\partial t^2}\right)-m_0\left(\frac{\partial^2 w_0}{\partial t^2}+B^2\frac{\partial^6 w_0}{\partial x^4\partial t^2}+2B\frac{\partial^4 w_0}{\partial x^2\partial t^2}\right)-k_w\frac{\partial^2 w_0}{\partial x^2}\right]=0\right.$$
$$A_{44}BE_{15}\frac{\partial^4 w_0}{\partial x^4}-D_{11}E_{31}\frac{\partial^2 w_0}{\partial x^2}-X_{11}\frac{\partial^2\Phi}{\partial x^2}+X_{33}\Phi=0 \quad (26a\text{-}b)$$

3. Solution Technique

In this section Navier solution method is used which reduces the partial differential equation (PDE) to an algebraic one as [48]

$$w_0(x,t)=y(x)W(t) \quad (27a)$$
$$\Phi(x,t)=y(x)\Omega(t) \quad (27b)$$

In which $y(x)$ is a fundamental mode shape, $W(t)$ and $\Omega(t)$ are temporary functions based on time. The mode shape which determines pivot boundary conditions is as

$$y(x)=\sin\left(\pi\frac{x}{L}\right) \quad (28)$$

Substituting Eq. (27) into Eq. (26), Eq. (26) reduces to an algebraic equation where to compute pivot boundary supports, Eq. (28) is employed. Thereafter, in order to present vibration frequencies a harmonic function is assumed as below

$$\Omega(t)=\exp(\omega_n t) \quad (29a)$$
$$W(t)=\exp(\omega_n t) \quad (29b)$$

In which ω_n corresponds to the complex frequency of the nanowire. The natural frequency is divided into two parts, real and imaginary as

$$\omega_n=\lambda+i\chi,\ i=\sqrt{-1} \quad (30)$$

In which λ is the real part and χ is the imaginary part of the complex frequency, respectively. The real part shows damping ratio for the model and the imaginary part represents natural frequency. Consequently, based on the given algorithm and some mathematical simplifying, the equation below can be obtained.

$$[K]\cdot\begin{Bmatrix}W(t)\\ \Omega(t)\end{Bmatrix}\cdot sin\left(\pi\frac{x}{L}\right)\cdot exp(\omega_n t)=0 \quad (31)$$

To compute the natural frequency of the piezo-visco-nanowire, a nontrivial solution can be done by vanishing determinant of the coefficients matrix ($det\left[K\right]=0$). After that, by calculating the obtained equation based on ω_n the numeric outcomes for the natural frequency can be shown (Appendix A).

4. Examples and Discussions

At this point, several samples are considered with which a crystal comparison between the current formulation and others is presented. Table 1 considers several references with various beam approaches. As it is found, the numerical outcomes of the present work are matched with those obtained by references. In addition, very good agreements are observed whenever the beam tends to be thinner with increasing its ratio of length to thickness. The reason is because at this condition the influence of shear deformations cannot be important and the results of the mentioned beam theories are close to one another. By this Table, the current formulation can be approved and so, the numerical outcomes can be further developed by changes in the essential variables. On the other hand, the mechanical and electrical quantities and properties of the employed nanowire can be seen at Table 2 which are found by the well-known references.

Table 1. Validations for nondimensional vibration frequencies.

$\Omega_n=\omega_n L^2\sqrt{\frac{\rho A}{EI}}$, $E=1TPa$, $\upsilon=0.3$, $h=1nm$

L/h	$(e_0a)^2$	Present	Timoshenko beam theory (TBT)		Sinusoidal beam theory (SBT)	
			[68]	[69]	[68]	[69]
5	0	9.2943	9.2740	9.2740	9.2752	9.2752
	1	8.8587	8.8477	8.8477	8.8488	8.8488
	2	8.4788	8.4752	8.4752	8.4763	8.4763
	3	8.1495	8.1461	8.1461	8.1472	8.1472
	4	7.8693	7.8526	7.8526	7.8536	7.8536
10	0	9.7209	9.7075	9.7075	9.7077	9.7077
	1	9.2666	9.2612	9.2612	9.2614	9.2614
	2	8.8857	8.8713	8.8713	8.8715	8.8715
	3	8.5483	8.5269	8.5269	8.5271	8.5271
	4	8.2320	8.2196	8.2196	8.2198	8.2198
20	0	9.8377	9.8281	9.8281	9.8282	9.8282
	1	9.3840	9.3763	9.3763	9.3764	9.3764
	2	8.9917	8.9816	8.9816	8.9816	8.9816
	3	8.6456	8.6328	8.6328	8.6329	8.6329
	4	8.3329	8.3218	8.3218	8.3218	8.3218

Table 2. The mechanical, electrical and geometrical characteristics of the piezo-nanowire [49]

Material	Mechanical and electrical Properties
$BaTiO_3$	Dielectric ($C/V.m$)
	$\kappa_{11}=5.64e-9$, $\kappa_{33}=6.35e-9$
	Piezoelectric (C/m^2)
	$e_{31}=-2.2$, $e_{15}=5.8$, $e_{33}=9.3$
	Elastic (GPa)
	$C_{11}=226$, $C_{13}=124$, $C_{33}=216$, $C_{44}=44.2$
	$\beta=L/d$ (Aspect ratio), $d=5$ nm, $\rho=5550$ kg/m^3, $k_w=1.13GPa$

According to Figs. 2, the changes in the parameter of the electric voltage can be seen versus small scale parameters' changes. It is evident from both figures the influences of changes in the outer voltage on frequency results of the system is insignificant. As a matter of fact, the nanowire used in the present study does not have a significant reaction to external electricity, although the influence is sufficiently large at such nanoscale. Perhaps it's because of its very low nanoscale thickness or its one dimensional manner. Furthermore, it is observed that increasing the nonlocal parameter in NSGT relation results in reduction of the natural frequency and regarding the second figure, the length scale parameter of the relation leads to increasing of the natural frequency. It can also be worth noting that in the case of both parameters which have the same values (e.g. value 1), the natural frequency of the nanowire in both figures will be in same values that are quite logical. In fact, this mode represents a local analysis, not taking the influences of small scale into account.

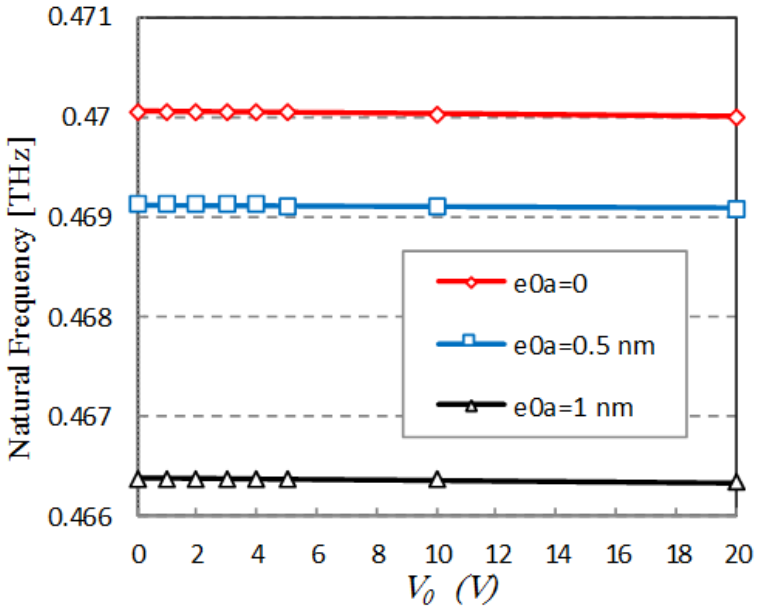

Fig. 2a. Effects of variations of the electric voltage versus nonlocal parameter on the natural frequencies ($\beta=5$, $l=1nm$, $g=5N.s/m$)

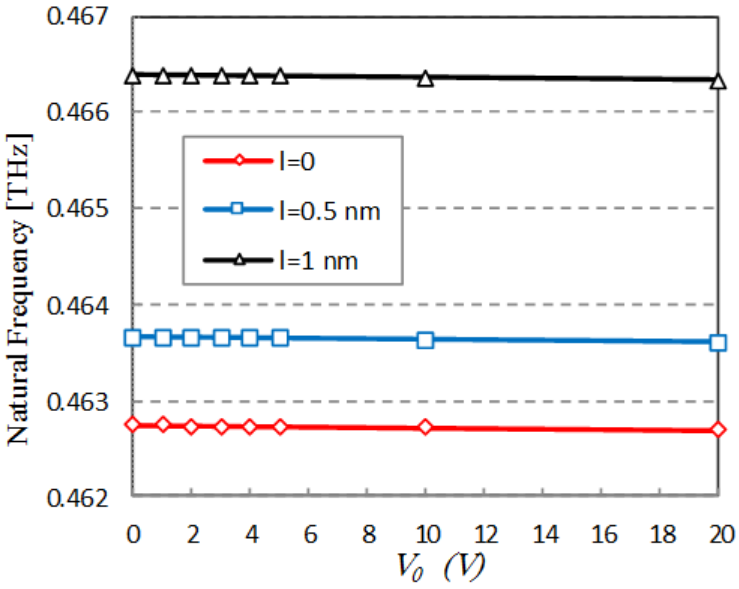

Fig. 2b. Effects of variations of the electric voltage versus length scale parameter on the natural frequencies ($\beta=5$, $e_0a=1nm$, $g=5N.s/m$)

Figure 3 exhibits the variation of the coefficient of internal viscosity of the nanowire against the nonlocal coefficient's variation. It is quite clear from the figure that the natural frequency is increased with increasing the viscoelastic coefficient. In fact, from a physical point of view, by increasing the coefficient, the nanowire's energy absorption is higher, and so the nanowire will have a larger frequency. Moreover, the frequency variations are linear and with a slight gradient. It can be concluded that for nanowires with very large lengths, the effect of viscosity is not remarkable. In Fig. 4, the effect of changes in the Winkler elastic foundation on the frequency results of the nanowire can be observed. In fact, after embedding the elastic base, the system provides greater frequencies. Such an increase is shown with a fairly significant gradient in the aforementioned figure. It can also be seen that changes in the viscosity of the nanowire do not affect the variation of the elastic base. The reason is as a result of the parallelism of results of the three viscosity coefficients in Fig. 4.

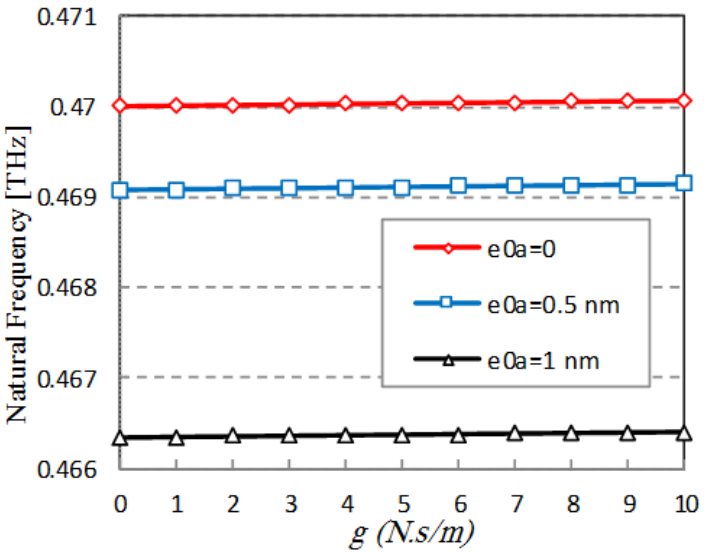

Fig. 3. Effects of variations of the viscoelastic coefficient versus nonlocal parameter on the natural frequencies ($V_0=5V$, $\beta=5$, $l=1nm$)

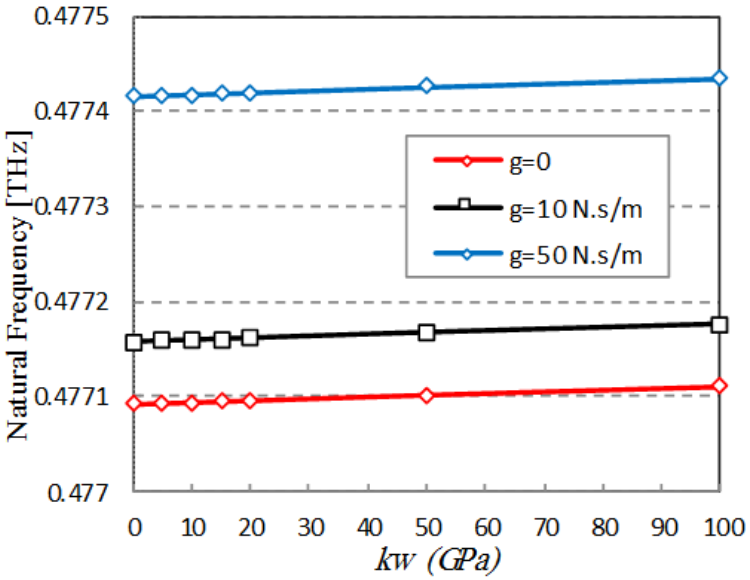

Fig. 4. Effects of variations of the Winkler parameter versus viscoelastic coefficient on the natural frequencies (V_0=5V, β=5, e_0a=1nm, l=2nm)

Figure 5 shows an important effect on nanowires. In fact, the physical nature of the nanowires is wires of very long lengths. For example, nanowires with a length to thickness ratio of 1,000 are also available. According to this figure, it can be seen that in large proportions of this coefficient, the small scale effect is completely unimportant. However, in small ratios of this factor, the effect of small scale will be larger. Additionally, increasing the aspect ratio to 7 will lead to a sharp decrease of vibration results for the nanostructure, and then the slope of the results will be mitigated. To the extent that it can be said, in very large quantities, the effect of the coefficient's changes does not affect the frequency results of the modeled system in the present study.

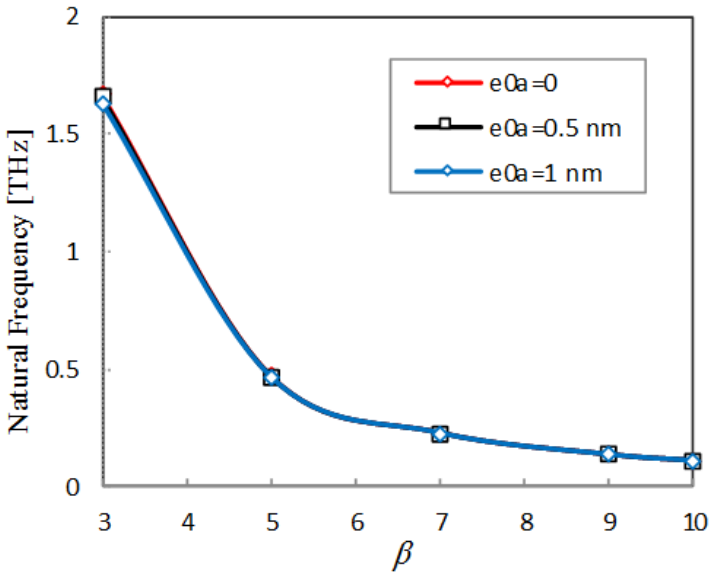

Fig. 5. Effects of variations of the aspect ratio versus nonlocal parameter on the natural frequencies (V_0=10V, g=5N.s/m, l=1nm)

5. Conclusions

In the study, a nanowire was embedded in an elastic substrate, and the electric field was assumed to be longitudinal. To analyze the effects of size-dependent, the nonlocal strain gradient theory was employed which has two variables. One parameter, known as nonlocal parameter, measures effects of quantum mechanics on the surface, and the second factor, known as the length scale one, measures the stiffness effects of the material by decreasing its size. The marked outcomes are listed below:

- Although the $BaTiO_3$ nanowire does not react remarkably to the external voltage, the influence is sufficiently large and cannot be neglected at nanoscale.
- Whilst the nanowire is very large, the effects of small scale and viscoelasticity cannot be considerable.
- The effect of increase of the external voltage on the nonlocal parameter is more than the length scale one.
- Increase of the viscoelastic parameter is further remarkable for lower values of the nonlocal parameter.

Appendix A:

$$K_{11}=\left\{\left[\left(1+g\omega_n\right)\left(D_{11}\left(\frac{\pi}{L}\right)^4+A_{44}B^2\left(-\left(\frac{\pi}{L}\right)^6\right)\right)\right]+N_x^E\left(B^2\left(-\left(\frac{\pi}{L}\right)^6\right)+2B\left(\frac{\pi}{L}\right)^4+\left(-\left(\frac{\pi}{L}\right)^2\right)\right)+\left(\omega_n\right)^2\times\right.$$
$$\left.\left[-I_m\left(-\left(\frac{\pi}{L}\right)^2\right)-m_0\left(1+B^2\left(\frac{\pi}{L}\right)^4+2B\left(-\left(\frac{\pi}{L}\right)^2\right)\right)\right]\right\}+\left\{-l^2\left[\left(1+g\omega_n\right)\left(D_{11}\left(-\left(\frac{\pi}{L}\right)^6\right)+A_{44}B^2\left(\frac{\pi}{L}\right)^8\right)\right]\right.$$
$$-k_w\left(-\left(\frac{\pi}{L}\right)^2\right)-\mu N_x^E\left(B^2\left(\frac{\pi}{L}\right)^8+2B\left(-\left(\frac{\pi}{L}\right)^6\right)+\left(\frac{\pi}{L}\right)^4\right)+\mu k_w\left(\frac{\pi}{L}\right)^4-\mu\left(\omega_n\right)^2\times$$
$$\left.\left[-I_m\left(\frac{\pi}{L}\right)^4-m_0\left(\left(-\left(\frac{\pi}{L}\right)^2\right)+B^2\left(-\left(\frac{\pi}{L}\right)^6\right)+2B\left(\frac{\pi}{L}\right)^4\right)\right]\right\}$$

$$K_{12}=\left(BE_{15}+E_{31}\right)\left(\frac{\pi}{L}\right)^2+l^2\left(BE_{15}+E_{31}\right)\left(\frac{\pi}{L}\right)^4$$

$$K_{21}=A_{44}E_{15}\left(\frac{\pi}{L}\right)^4-D_{11}E_{31}\left(-\left(\frac{\pi}{L}\right)^2\right)$$

$$K_{22}=-X_{11}\left(-\left(\frac{\pi}{L}\right)^2\right)+X_{33}$$

Acknowledgments

The authors thank to the reviewers for their valuable comments which lead to improving the manuscript.

References

[1] Rao, C. N. R., Govindaraj, A., Nanotubes and Nanowires. *First Publishing, UK, R. S. C. Publication*, 2005.

[2] Hu, J., Odom, T. W., Lieber, C. M., Chemistry and Physics in One Dimension: Synthesis and Properties of Nanowires and Nanotubes. *Accounts of Chemical Research*, 32, 435-445, 1999.

[3] Lupu, N., Nanowires Science and Technology. *First Publishing, India, Intech*, 2010.

[4] Wang, Z. L., Nanowires and Nanobelts: Materials Properties and Devices, Nanowires and Nanobelts of Functional Materials. *First printing, USA, Springer*, 2006.

[5] Kiani, K., Magneto-elasto-dynamic analysis of an elastically confined conducting nanowire due to an axial magnetic shock. *Physics Letters A*, 376, 1679–1685, 2012.

[6] Kiani, K., Dynamic interactions between double current-carrying nanowires immersed in a longitudinal magnetic field: Novel integro-surface energy-based models. *International Journal of Engineering Science*, 107, 98–133, 2016.

[7] Pishkenari, H. N., Afsharmanesh, B., Tajaddodianfar, F., Continuum models calibrated with atomistic simulations for the transverse vibrations of silicon nanowires. *International Journal of Engineering Science*, 100, 8–24, 2016.

[8] Fu, Y., Zhang, P., Buckling and vibration of core–shell nanowires with weak interfaces. *Mechanics Research Communications*, 37, 622–626, 2010.

[9] Kiani, K., Surface effect on free transverse vibrations and dynamic instability of current-carrying nanowires in the presence of a longitudinal magnetic field. *Physics Letters A*, 378, 1834–1840, 2014.

[10] Gongbai, C., Yunfei, Ch., Jiwei, J., Yuelin, W., Harmonic behavior of silicon nanowire by molecular dynamics. *Mechanics Research Communications*, 34, 503–507, 2007.

[11] Zhoua, J., Wanga, Zh., Grotsb, A., Heb, X., Electric field drives the nonlinear resonance of a piezoelectric nanowire. *Solid State Communications*, 144, 118–123, 2007.

[12] Zhang, Y. Q., Pang, M., Chen, W. Q., Transverse vibrations of embedded nanowires under axial compression with high-order surface stress effects. *Physica E*, 66, 238–244, 2015

[13] Li, X.-F., Wang, B.-L., Tang, G.-J., Lee, K.-Y., Size effect in transverse mechanical behavior of one-dimensional nanostructures. *Physica E*, 44, 207–214, 2011.

[14] Su, G.-Y., Li, Y.-X., Li, X.-Y., Muller, R., Free and forced vibrations of nanowires on elastic substrates. *International Journal of Mechanical Sciences*, 138-139, 62-73, 2018.

[15] Tourki Samaei, A., Gheshlaghi, B., Wang, G.-F., Frequency analysis of piezoelectric nanowires with surface effects. *Current Applied Physics*, 13, 2098-2102, 2013.

[16] Gheshlaghi, B., Hasheminejad, S. M., Vibration analysis of piezoelectric nanowires with surface and small scale effects. *Current Applied Physics*, 12, 1096-1099, 2012.

[17] Kiani, K., Forced vibrations of a current-carrying nanowire in a longitudinal magnetic field accounting for both surface energy and size effects. *Physica E: Low-Dimensional Systems and Nanostructures*, 63, 27-35, 2014.

[18] Kiani, K., Stability and vibrations of doubly parallel current-carrying nanowires immersed in a longitudinal magnetic field. *Physics Letters A*, 379, 348–360, 2015.

[19] Kiani, K., A refined integro-surface energy-based model for vibration of magnetically actuated doublenanowire- systems carrying electric current. *Physica E: Low-Dimensional Systems and Nanostructures*, 86, 225-236, 2017.

[20] Mercan, K., Numanoglu, H. M., Akgöz, B., Demir, C., & Civalek, Ö., Higher order continuum theories for buckling response of silicon carbide nanowires (SiCNWs) on elastic matrix. *Archive of Applied Mechanics*, 87, 1797-1814, 2017.

[21] Mercan, K., & Civalek, Ö., Modal Analysis of Micro and Nanowires Using Finite Element Softwares. *International Journal of Engineering & Applied Sciences*, 10, 291-304, 2018.

[22] Numanoglu, H. M., Mercan, K., & Civalek, Ö., Frequency and mode shapes of Au nanowires using the continuous beam models. *International Journal of Engineering and Applied Sciences*, 4, 55-61, 2017.

[23] Akgöz, B., and Civalek, Ö., A size-dependent shear deformation beam model based on the strain gradient elasticity theory. *International Journal of Engineering Science*, 70, 1-14, 2013.

[24] Avcar, M., Free vibration of imperfect sigmoid and power law functionally graded beams. *Steel and Composite Structures*, 30, 603-615, 2019.

[25] Avcar, M., Effects of rotary inertia shear deformation and non-homogeneity on frequencies of beam. *Structural Engineering and Mechanics*, 55, 871-884, 2015.

[26] Avcar, M., Free vibration analysis of beams considering different geometric characteristics and boundary condition. *International Applied Mechanics*, 4, 94-100, 2014.

[27] Numanoglu, H. M., Akgöz, B., Civalek, Ö., On dynamic analysis of nanorods. *International Journal of Engineering Science*, 130, 33-50, 2018.

[28] Ufuk, G., Aydogdu, M., Noncoaxial vibration and buckling analysis of embedded double-walled carbon nanotubes by using doublet mechanics. *Composites Part B: Engineering*, 137, 60-73, 2018.

[29] Demir, C., Civalek, Ö., On the analysis of microbeams. *International Journal of Engineering Science*, 121, 14–33, 2017.

[30] Zhang, B., He, Y., Liu, D., Gan, Z., Shen, L., Non-classical Timoshenko beam element based on the strain gradient elasticity theory. *Finite Elements in Analysis and Design*, 79, 22-39, 2014.

[31] Mercan, K., Civalek, Ö., DSC method for buckling analysis of boron nitride nanotube (BNNT) surrounded by an elastic matrix. *Composite Structures*, 143, 300–309, 2016.

[32] Barretta, R. et al., A higher-order Eringen model for Bernoulli–Euler nanobeams. *Archive of Applied Mechanics*, 86, 483–495, 2016.

[33] Akgöz, B, Civalek Ö., Effects of thermal and shear deformation on vibration response of functionally graded thick composite microbeams. *Composites Part B: Engineering*, 129, 77-87, 2017.

[34] Mercan, K., Civalek, Ö., Buckling analysis of Silicon carbide nanotubes (SiCNTs) with surface effect and nonlocal elasticity using the method of HDQ. *Composites Part B*, 114, 34-45, 2017.

[35] Rahmani, O., Refaeinejad, V., Hosseini, S. A. H., Assessment of various nonlocal higher order theories for the bending and buckling behavior of functionally graded nanobeams. *Steel & Composite Structures, An International Journal*, 23, 339-350, 2014.

[36] Akgöz, B., Civalek, Ö., Buckling analysis of cantilever carbon nanotubes using the strain gradient elasticity and modified couple stress theories. *Journal of Computational and Theoretical Nanoscience*, 8, 1821-1827, 2011.

[37] Demir, C., Mercan, K., Civalek, Ö., Determination of critical buckling loads of isotropic, FGM and laminated truncated conical panel. *Composites Part B*, 94, 1-10, 2016.

[38] Civalek, Ö., Free vibration of carbon nanotubes reinforced (CNTR) and functionally graded shells and plates based on FSDT via discrete singular convolution method. *Composites Part B: Engineering*, 111, 45–59, 2017.

[39] Akgöz, B., Civalek, Ö., Nonlinear vibration analysis of laminated plates resting on nonlinear two parameters elastic foundations. *Steel and Composite Structures*, 11, 403–421, 2011.

[40] Thai, H. T., Kim, S. E., A review of theories for the modeling and analysis of functionally graded plates and shells. *Composite Structures*, 128, 70–86, 2015.

[41] Civalek, Ö., Acar M. H., Discrete singular convolution method for the analysis of Mindlin plates on elastic foundations. *International Journal of Pressure Vessels and Piping*, 84, 527–535, 2007.

[42] Shirmohammadi, F., Bahrami, S., Dynamic response of circular and annular circular plates using spectral element method. *Applied Mathematical Modelling*, 53, 156–166, 2018.

[43] Mercan, K., Civalek, Ö., DSC method for buckling analysis of boron nitride nanotube (BNNT) surrounded by an elastic matrix. *Composite Structures*, 143, 300–309, 2016.

[44] Civalek, Ö., Demir, Ç., Bending analysis of microtubules using nonlocal Euler–Bernoulli beam theory. *Applied Mathematical Modelling*, 35, 2053-2067, 2011.

[45] Demir, Ç., Civalek, Ö., Akgöz, B., Free vibration analysis of carbon nanotubes based on shear deformable beam theory by discrete singular convolution technique. *Mathematical and Computational applications*, 15, 57-65, 2010.

[46] Demir, Ç., Civalek, Ö., Akgöz, B., Free vibration analysis of carbon nanotubes based on shear deformable beam theory by discrete singular convolution technique. *Mathematical and Computational applications*, 15, 57-65, 2010.

[47] Malikan, M., Electro-mechanical shear buckling of piezoelectric nanoplate using modified couple stress theory based on simplified first order shear deformation theory. *Applied Mathematical Modelling*, 48, 196-207, 2017.

[48] Malikan, M., Nguyen, V. B., Tornabene, F., Damped forced vibration analysis of single-walled carbon nanotubes resting on viscoelastic foundation in thermal environment using nonlocal strain gradient theory, *Engineering Science and Technology, an International Journal*, 21, 778-786, 2018.

[49] Malikan, M., Nguyen, V. B., Buckling analysis of piezo-magnetoelectric nanoplates in hygrothermal environment based on a novel one variable plate theory combining with higher-order nonlocal strain gradient theory. *Physica E: Low-Dimensional Systems and Nanostructures*, 102, 8-28, 2018.

[50] Malikan, M., Temperature influences on shear stability of a nanosize plate with piezoelectricity effect. *Multidiscipline Modeling in Materials and Structures*, 14, 125-142, 2018.

[51] Malikan, M., Electro-thermal buckling of elastically supported double-layered piezoelectric nanoplates affected by an external electric voltage. *Multidiscipline Modeling in Materials and Structures*, 15, 50-78, 2019.

[52] Malikan, M., Buckling analysis of a micro composite plate with nano coating based on the modified couple stress theory. *Journal of Applied and Computational Mechanics*, 4, 1–15, 2018.

[53] Malikan, M., On the buckling response of axially pressurized nanotubes based on a novel nonlocal beam theory. *Journal of Applied and Computational Mechanics*, 5, 103-112, 2019.

[54] Malikan, M., Jabbarzadeh, M., Dastjerdi, Sh., Non-linear Static stability of bi-layer carbon nanosheets resting on an elastic matrix under various types of in-plane shearing loads in thermo-elasticity using nonlocal continuum. *Microsystem Technologies*, 23, 2973–2991, 2017.

[55] Malikan, M., Nguyen, V.B., A novel one-variable first-order shear deformation theory for biaxial buckling of a size-dependent plate based on the Eringen′s nonlocal differential law. *World Journal of Engineering*, 15, 633-645, 2018.

[56] Malikan, M., Sadraee Far, M. N., Differential quadrature method for dynamic buckling of graphene sheet coupled by a viscoelastic medium using neperian frequency based on

nonlocal elasticity theory. *Journal of Applied and Computational Mechanics*, 4, 147-160, 2018.

[57] Malikan, M., Tornabene, F., Dimitri, R., Nonlocal three-dimensional theory of elasticity for buckling behavior of functionally graded porous nanoplates using volume integrals. *Materials Research Express*, 5, 095006, 2018.

[58] Malikan, M., Nguyen, V.B., Tornabene, F., Electromagnetic forced vibrations of composite nanoplates using nonlocal strain gradient theory. *Materials Research Express*, 5, 075031, 2018.

[59] Malikan, M., Dimitri, R., Tornabene, F., Effect of Sinusoidal Corrugated Geometries on the Vibrational response of Viscoelastic Nanoplates. *Applied Sciences*, 8, 1432, 2018.

[60] Malikan, M., Nguyen, V.B., Dimitri, R., Tornabene, F., Dynamic modeling of non-cylindrical curved viscoelastic single-walled carbon nanotubes based on the second gradient theory. *Materials Research Express*, 6, 075041, 2019.

[61] Malikan, M., Dimitri, R., Tornabene, F., Transient response of oscillated carbon nanotubes with an internal and external damping. *Composites Part B: Engineering*, 158, 198-205, 2019.

[62] Malikan, M., Analytical predictions for the buckling of a nanoplate subjected to non-uniform compression based on the four-variable plate theory. *Journal of Applied and Computational Mechanics*, 3, 217-228, 2017.

[63] Malikan, M., Dastjerdi, Sh., Analytical buckling of FG nanobeams on the basis of a new one variable first-order shear deformation beam theory. *International Journal of Engineering & Applied Sciences*, 10, 21-34, 2018.

[64] Golmakani, M. E., Malikan, M., Sadraee Far, M. N., Majidi, H. R., Bending and buckling formulation of graphene sheets based on nonlocal simple first order shear deformation theory, *Materials Research Express*, 5, 065010, 2018.

[65] Malikan, M., Dimitri, R., Tornabene, F., Thermo-resonance analysis of an excited graphene sheet using a new approach, *International Journal of Engineering & Applied Sciences*, 10, 190-206, 2018.

[66] Lim, C. W., Zhang, G., Reddy, J. N., A Higher-order nonlocal elasticity and strain gradient theory and Its Applications in wave propagation. *Journal of the Mechanics and Physics of Solids*, 78, 298-313, 2015.

[67] Lei, Y., Adhikari, S., Friswell, M. I., Vibration of nonlocal Kelvin–Voigt viscoelastic damped Timoshenko beams. *International Journal of Engineering Science*, 66–67, 1–13, 2013.

[68] Thai, H. T., A nonlocal beam theory for bending, buckling, and vibration of nanobeams, *International Journal of Engineering Science*, 52, 56–64, 2012.

[69] Lu, L., Guo, X., Zhao, J., Size-dependent vibration analysis of nanobeams based on the nonlocal strain gradient theory. *International Journal of Engineering Science*, 116, 12–24, 2017.

International Journal of Engineering & Applied Sciences (IJEAS)
Vol.11, Issue 2 (2019) 387-400
http://dx.doi.org/10.24107/ijeas.569798
Int J Eng Appl Sci 11(2) (2019) 387-400

Finite Element Model of Functionally Graded Nanobeam for Free Vibration Analysis

Büşra Uzun [a], Mustafa Özgür Yaylı [b]*

[a,b] *Bursa Uludag University, Civil Engineering Department*
Division of Mechanics, Bursa-TURKIYE

[*] *E-mail address*: buzun@uludag.edu.tr [a*], ozguryayli@uludag.edu.tr [b]

ORCID numbers of authors:
0000-0002-7636-7170[a], 0000-0003-2231-170X[b]*

Received date: 24.05.2019
Accepted date: 12.06.2019

Abstract

In the present study, free vibration of functionally graded (FG) nanobeam is investigated. The variation of material properties is assumed in the thickness direction according to the power law. FG nanobeam is modeled as Euler-Bernoulli beam with different boundary conditions and investigated based on Eringen's nonlocal elasticity theory. Governing equations are derived via Hamilton principle. Frequency values are found by using finite element method. FG nanobeam is composed of silicon carbide (SiC) and stainless steel (SUS304). The effects of dimensionless small-scale parameters (e_0a/L), power law exponent (k) and boundary conditions on frequencies are examined for FG nanobeam.

Keywords: Functionally graded nanobeam, nonlocal elasticity theory, free vibration, finite element method

1. Introduction

Functionally graded materials (FGMs) are defined as special composites which material properties change continuously along with direction of the material. FGMs are mostly composed of ceramic and metal. Thus the ceramic can resist high temperature in thermal environments, while the metal can reduce the stress occurring on the ceramic surface at the earlier case of cooling. FGMs are utilized in various applications such as aviation, mechanical, electronics, nuclear, optics, chemical, biomedicine and civil engineering [1-2].

The classical continuum theories lose their validity when the dimensions are reduced because they lack internal/additional material small-scale parameters. For this reason, some researchers have been used some higher order theories that take into account small-scale effect analysis of micro and nano structures [3-5]. Among higher order theories, nonlocal elasticity theory [6] have been widely studied recently [7-21]. Ebrahimi et al. [2] presented the applicability of differential transformation method (DTM) in investigations on vibrational characteristics of FG size-dependent nanobeams. Civalek and Demir [22] developed elastic beam model using nonlocal elasticity theory and Euler–Bernoulli beam theory for the bending

analysis of microtubules (MTs). Kadıoğlu and Yaylı [23] studied buckling analysis of a nano sized beam by using Timoshenko beam theory and Eringen's nonlocal elasticity theory. Zargaripoor et al. [24] investigated free vibration of functionally graded nanoplate by using Eringen's nonlocal theory.

In this study, vibration characteristics of FG nanobeams are investigated. The variation of material properties is assumed in the thickness direction based on the power law. FG nanobeam is composed of silicon carbide (SiC) and stainless steel (SUS304). Governing equations are derived via Hamilton principle. The vibration behaviours of SiC/SUS304 FG nanobeam with simply-supported (S-S) and clamped-clamped (C-C) boundary conditions are analyzed using nonlocal finite element formulation. The effects of small-scale parameters (e_0a/L), power law exponents (k) and boundary conditions on frequencies are examined for FG nanobeam.

2. Functionally Graded Euler-Bernoulli Beam

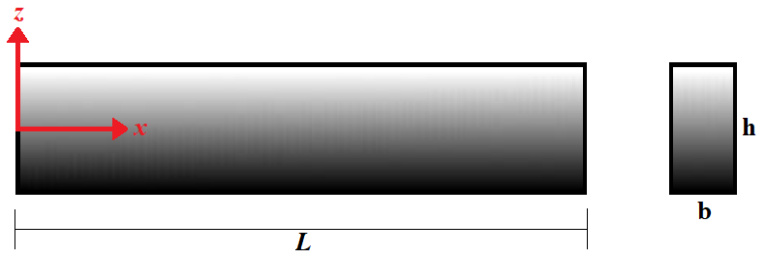

Fig. 1. Ilustration of FG beam

L, b and h are length, width and thickness of the FG beam, respectively. The material properties of the beam are assumed to vary continuously in the thickness direction. The effective material property of FG beam is expressed by the power law as follows [9]

$$P(z) = (P_U - P_L)\left(\frac{z}{h} + \frac{1}{2}\right)^k + P_L \tag{1}$$

Here $P(z)$ is the effective material property of the beam, P_U and P_L are the material property at the upper and lower surfaces of the beam, k is the power law exponent (non-negative variable parameter). $P(z)$ indicates to the properties of the beam components such as the elastic module (E), density (ρ) etc. and can be transformed into the following forms

$$E(z) = (E_U - E_L)\left(\frac{z}{h} + \frac{1}{2}\right)^k + E_L \tag{2}$$

$$\rho(z) = (\rho_U - \rho_L)\left(\frac{z}{h} + \frac{1}{2}\right)^k + \rho_L \tag{3}$$

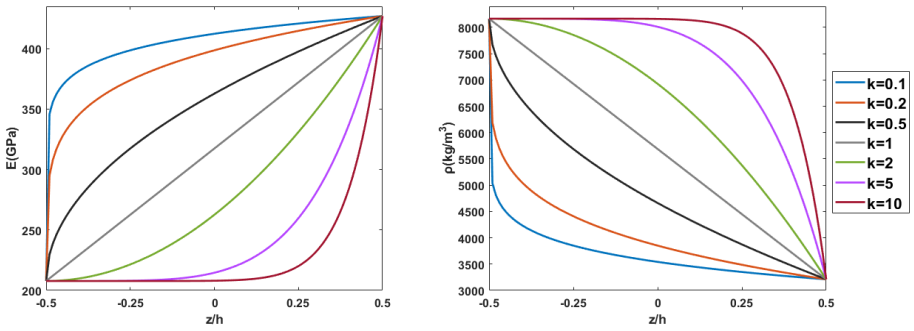

Fig. 2. The variation of material properties through the thickness direction

The displacements for Euler-Bernoulli beam can be written as follows [13]

$$u_1(x,z,t) = u(x,t) - z\frac{\partial w(x,t)}{\partial x} \tag{4a}$$

$$u_2(x,z,t) = 0 \tag{4b}$$

$$u_3(x,z,t) = w(x,t) \tag{4c}$$

Here u_1, u_2 and u_3 are the displacements in the x, y, z directions, respectively. u and w denote longitudinal and transverse displacements of any point on the neutral axis, respectively. Strains of the Euler-Bernoulli beam as follows

$$\varepsilon_{xx} = \frac{\partial u(x,t)}{\partial x} - z\frac{\partial^2 w(x,t)}{\partial x^2},\ \varepsilon_{xy} = \varepsilon_{yx} = \varepsilon_{xz} = \varepsilon_{zx} = \varepsilon_{yy} = \varepsilon_{yz} = \varepsilon_{zy} = \varepsilon_{zz} = 0 \tag{5}$$

ε_{xx} is the non-zero only strain component. Stress, normal force and moment expressions for the functionally graded beam are written as follows

$$\sigma_{xx} = E(z)\varepsilon_{xx} \tag{6}$$

$$N = A_1\frac{\partial u}{\partial x} - B_1\frac{\partial^2 w}{\partial x^2},\ M = B_1\frac{\partial u}{\partial x} - D_1\frac{\partial^2 w}{\partial x^2} \tag{7}$$

A_1, B_1 ve D_1 are expressed as

$$A_1 = \int_A E(z)dA,\ B_1 = \int_A E(z)zdA,\ D_1 = \int_A E(z)z^2dA \tag{8}$$

The Hamilton principle to be used to obtain equations of motion is expressed as follows [25]

$$\int_0^T (\delta S - \delta T)dt = 0 \tag{9}$$

Where S and T are the strain energy and kinetic energy, respectively. S and T for an element which has volume V and length L is as below

$$S = \frac{1}{2}\int_V \sigma_{xx}\varepsilon_{xx}dV \tag{10}$$

$$T = \frac{1}{2}\int_V \rho(z)\left(\left(\frac{\partial u_1}{\partial t}\right)^2 + \left(\frac{\partial u_2}{\partial t}\right)^2 + \left(\frac{\partial u_3}{\partial t}\right)^2\right)dV \tag{11}$$

The first variation of the strain and kinetic energy are obtained as follows

$$\begin{aligned}\delta\int_0^T Sdt &= \int_0^T\int_0^L \left(N\delta\left(\frac{\partial u}{\partial x}\right) - M\delta\left(\frac{\partial^2 w}{\partial x^2}\right)\right)dxdt \\ &= \int_0^T\int_0^L \left(\left(A_1\frac{\partial u}{\partial x} - B_1\frac{\partial^2 w}{\partial x^2}\right)\delta\left(\frac{\partial u}{\partial x}\right) - \left(B_1\frac{\partial u}{\partial x} - D_1\frac{\partial^2 w}{\partial x^2}\right)\delta\left(\frac{\partial^2 w}{\partial x^2}\right)\right)dxdt\end{aligned} \tag{12}$$

$$\delta\int_0^T Tdt = \int_0^T\int_0^L \left(I_0\left(\frac{\partial u}{\partial t}\delta\left(\frac{\partial u}{\partial t}\right) + \frac{\partial w}{\partial t}\delta\left(\frac{\partial w}{\partial t}\right)\right) - I_1\left(\frac{\partial u}{\partial t}\delta\left(\frac{\partial^2 w}{\partial x\partial t}\right) + \frac{\partial^2 w}{\partial x\partial t}\delta\left(\frac{\partial u}{\partial t}\right)\right) + I_2\frac{\partial^2 w}{\partial x\partial t}\delta\left(\frac{\partial^2 w}{\partial x\partial t}\right)\right)dxdt \tag{13}$$

Here I_0, I_1 and I_2 are expressed as

$$I_0 = \int_A \rho(z)dA,\ I_1 = \int_A \rho(z)zdA,\ I_2 = \int_A \rho(z)z^2dA \tag{14}$$

Substituting Equations (12) and (13) into Equation (9), we obtain the equilibrium equations from the Euler-Lagrange equation as follows

$$\delta u : \frac{\partial N}{\partial x} = I_0 \frac{\partial^2 u}{\partial t^2} - I_1 \frac{\partial^3 w}{\partial x \partial t^2} \tag{15}$$

$$\delta w : \frac{\partial^2 M}{\partial x^2} = I_0 \frac{\partial^2 w}{\partial t^2} + I_1 \frac{\partial^3 u}{\partial x \partial t^2} - I_2 \frac{\partial^4 w}{\partial x^2 \partial t^2} \tag{16}$$

3. Nonlocal Functionally Graded Nanobeam

The nonlocal constitutive formulation is [6]

$$\left[1-\left(e_0 a\right)^2 \nabla^2\right]\sigma_{ij} = C_{ijkl}\varepsilon_{kl} \tag{17}$$

Where σ_{ij} is the stress tensor, C_{ijkl} is the fourth-order elastic module tensor, ε_{kl} is the strain tensor, e_0 is a material constant which is determined experimentally, a is the internal characteristic length. For Euler–Bernoulli FG nanobeam, Equation (17) can be rewritten as

$$\sigma_{xx} - \left(e_0 a\right)^2 \frac{\partial^2 \sigma_{xx}}{\partial x^2} = E(z)\varepsilon_{xx} \tag{18}$$

Integrating Equation (18) over the cross-section area, we obtain the axial force-strain relation as

$$N - (e_0 a)^2 \frac{\partial^2 N}{\partial x^2} = A_1 \frac{\partial u}{\partial x} - B_1 \frac{\partial^2 w}{\partial x^2} \tag{19}$$

Multiplying Equation (18) by z and integrating over the cross-section area, we get the moment-curvature relation as

$$M-(e_0a)^2\frac{\partial^2 M}{\partial x^2}=B_1\frac{\partial u}{\partial x}-D_1\frac{\partial^2 w}{\partial x^2} \tag{20}$$

Differentiating Equation (15) with respect to x, then substituting Equation (19) we obtain Equation (21). And substituting Equation (16), we obtain Equation (22).

$$N=A_1\frac{\partial u}{\partial x}-B_1\frac{\partial^2 w}{\partial x^2}+(e_0a)^2\left(I_0\frac{\partial^3 u}{\partial x\partial t^2}-I_1\frac{\partial^4 w}{\partial x^2\partial t^2}\right) \tag{21}$$

$$M=B_1\frac{\partial u}{\partial x}-D_1\frac{\partial^2 w}{\partial x^2}+(e_0a)^2\left(I_0\frac{\partial^2 w}{\partial t^2}+I_1\frac{\partial^3 u}{\partial x\partial t^2}-I_2\frac{\partial^4 w}{\partial x^2\partial t^2}\right) \tag{22}$$

4. Finite Element Formulation

The variational statement of FG Euler–Bernoulli nanobeam has the following form

$$\int_0^T\int_0^L\left(\begin{array}{l}\left(A_1\frac{\partial u}{\partial x}\delta\left(\frac{\partial u}{\partial x}\right)-B_1\frac{\partial^2 w}{\partial x^2}\delta\left(\frac{\partial u}{\partial x}\right)+(e_0a)^2\left(I_0\frac{\partial^3 u}{\partial x\partial t^2}\delta\left(\frac{\partial u}{\partial x}\right)-I_1\frac{\partial^4 w}{\partial x^2\partial t^2}\delta\left(\frac{\partial u}{\partial x}\right)\right)\right)\\ -\left(\begin{array}{l}B_1\frac{\partial u}{\partial x}\delta\left(\frac{\partial^2 w}{\partial x^2}\right)-D_1\frac{\partial^2 w}{\partial x^2}\delta\left(\frac{\partial^2 w}{\partial x^2}\right)\\ +(e_0a)^2\left(I_0\frac{\partial^2 w}{\partial t^2}\delta\left(\frac{\partial^2 w}{\partial x^2}\right)+I_1\frac{\partial^3 u}{\partial x\partial t^2}\delta\left(\frac{\partial^2 w}{\partial x^2}\right)-I_2\frac{\partial^4 w}{\partial x^2\partial t^2}\delta\left(\frac{\partial^2 w}{\partial x^2}\right)\right)\end{array}\right)\\ -\left(I_0\left(\frac{\partial u}{\partial t}\delta\left(\frac{\partial u}{\partial t}\right)+\frac{\partial w}{\partial t}\delta\left(\frac{\partial w}{\partial t}\right)\right)-I_1\left(\frac{\partial u}{\partial t}\delta\left(\frac{\partial^2 w}{\partial x\partial t}\right)+\frac{\partial^2 w}{\partial x\partial t}\delta\left(\frac{\partial u}{\partial t}\right)\right)+I_2\frac{\partial^2 w}{\partial x\partial t}\delta\left(\frac{\partial^2 w}{\partial x\partial t}\right)\right)\end{array}\right)dxdt \tag{23}$$

ϕu and ϕw are the interpolation shape functions and they are expressed as below

$$[\phi_u]=\left[1-\frac{x}{L}\quad\frac{x}{L}\right] \tag{24}$$

$$[\phi_w]=\left[1-\frac{3x^2}{L^2}+\frac{2x^3}{L^3}\quad x-\frac{2x^2}{L}+\frac{x^3}{L^2}\quad\frac{3x^2}{L^2}-\frac{2x^3}{L^3}\quad-\frac{x^2}{L}+\frac{x^3}{L^2}\right] \tag{25}$$

The stiffness matrices (K_u, K_{uw}, K_w), the classical mass matrices (M_u^c, M_{uw}^c, M_w^c) and the nonlocal mass matrices (M_u^{nl}, M_{uw}^{nl}, M_w^{nl}) are obtained using Equations (23)-(25) as follows

$$K_u=\int_0^L A_1\left([\phi_u]'\right)^T[\phi_u]'\,dx \tag{26}$$

$$K_{uw} = -\left(\int_0^L B_1 \left([\phi_w]'' \right)^T [\phi_u]' \, dx + \int_0^L B_1 \left([\phi_u]' \right)^T [\phi_w]'' \, dx \right) \tag{27}$$

$$K_w = \int_0^L D_1 \left([\phi_w]'' \right)^T [\phi_w]'' \, dx \tag{28}$$

$$M_u^c = \int_0^L I_0 \left([\phi_u] \right)^T [\phi_u] dx \tag{29}$$

$$M_{uw}^c = -\left(\int_0^L I_1 \left([\phi_u] \right)^T [\phi_w]' \, dx + \int_0^L I_1 \left([\phi_w]' \right)^T [\phi_u] dx \right) \tag{30}$$

$$M_w^c = \int_0^L I_0 \left([\phi_w] \right)^T [\phi_w] dx + \int_0^L I_2 \left([\phi_w]' \right)^T [\phi_w]' dx \tag{31}$$

$$M_u^{nl} = (e_0 a)^2 \int_0^L I_0 \left([\phi_u]' \right)^T [\phi_u]' \, dx \tag{32}$$

$$M_{uw}^{nl} = -\left((e_0 a)^2 \int_0^L I_1 \left([\phi_u]' \right)^T [\phi_w]'' \, dx + (e_0 a)^2 \int_0^L I_1 \left([\phi_w]'' \right)^T [\phi_u]' dx \right) \tag{33}$$

$$M_w^{nl} = -(e_0 a)^2 \int_0^L I_0 \left([\phi_w] \right)^T \frac{\partial^2 [\phi_w]}{\partial x^2} dx + (e_0 a)^2 \int_0^L I_2 \left(\frac{\partial^2 [\phi_w]}{\partial x^2} \right)^T \frac{\partial^2 [\phi_w]}{\partial x^2} dx \tag{34}$$

The frequencies of FG nanobeam are found as follows

$$\left| K - \omega^2 M \right| = 0 \tag{35}$$

Here ω is frequency. *K* and *M* are total stiffness and mass matrices and given in Equations (36) and (37)

$$K = K_u + K_w + K_{uw} \tag{36}$$

$$M = M_u^c + M_{uw}^c + M_w^c + M_u^{nl} + M_{uw}^{nl} + M_w^{nl} \tag{37}$$

5. Numerical Results for Free Vibration of FG Nanobeam

In this section frequency values of SiC/SUS304 FG nanobeam are obtained with various dimensionless small-scale parameters (e_0a/L), power law exponents (k) and different boundary conditions such as S-S and C-C. The bottom surface of the beam is pure metal (SUS304) whereas the top surface of the beam is pure ceramic (SiC). Mechanical properties of nanobeam constituents are given in Table 1. Geometrical properties of the FG nanobeam are: b (width) = 100 nm, h (thickness) = 200 nm and L (length) = 10000 nm.

Table 1. Properties of FG nanobeams constituents [26]

	Properties	
	E (Gpa)	**ρ (kg/m^3)**
Silicon Carbide (SiC)	427	3210
Stainless Steel (SUS304)	207.78	8166

The frequency values obtained from the analyses of S-S FG nanobeam and C-C FG nanobeam with various e_0a/L ranging from 0 to 0.5 and various k ranging from 0 to 10 are presented in Table 2 and Table 3, respectively.

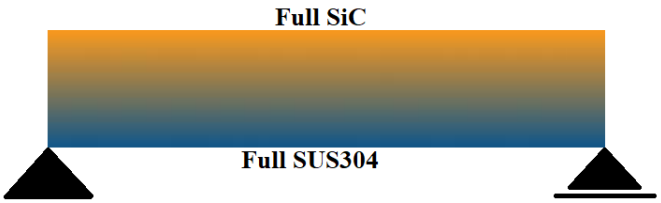

Fig. 3. Functionally graded S-S nanobeam

Table 2. Variation of first five frequencies (MHz) of FG nanobeam with k and e_0a/L (S-S)

k	**ω (MHz)**	**e_0a/L**					
		0	**0.1**	**0.2**	**0.3**	**0.4**	**0.5**
0	**ω_1**	10.4580	9.9772	8.8551	7.6106	6.5120	5.6163
	ω_2	41.8114	35.4031	26.0350	19.5949	15.4576	12.6820
	ω_3	93.9986	68.4054	44.0524	31.3427	24.1004	19.5126
	ω_4	166.9175	103.9357	61.7090	42.7962	32.5689	26.2355
	ω_5	260.4264	139.8566	78.9911	54.0604	40.9330	32.8930
0.2	**ω_1**	8.8233	8.4177	7.4710	6.4210	5.4941	4.7384
	ω_2	35.2750	29.8685	21.9649	16.5316	13.0411	10.6994
	ω_3	79.3007	57.7093	37.1643	26.4418	20.3320	16.4616
	ω_4	140.8103	87.6793	52.0573	36.1025	27.4749	22.1321
	ω_5	219.6787	117.9739	66.6317	45.6018	34.5284	27.7464
2	**ω_1**	6.1069	5.8262	5.1709	4.4442	3.8026	3.2796
	ω_2	24.4163	20.6741	15.2035	11.4427	9.0266	7.4058
	ω_3	54.8939	39.9478	25.7260	18.3037	14.0743	11.3951
	ω_4	97.4831	60.7005	36.0393	24.9938	19.0209	15.3221
	ω_5	152.1054	81.6851	46.1358	31.5747	23.9074	19.2116
5	**ω_1**	5.5038	5.2508	4.6602	4.0052	3.4271	2.9557

	ω_2	22.0051	18.6325	13.7021	10.3127	8.1352	6.6745
	ω_3	49.4742	36.0037	23.1861	16.4965	12.6848	10.2701
	ω_4	87.8615	54.7093	32.4822	22.5269	17.1435	13.8098
	ω_5	137.0985	73.6259	41.5840	28.4595	21.5487	17.3161
10	ω_1	5.1688	4.9312	4.3766	3.7615	3.2185	2.7758
	ω_2	20.6658	17.4984	12.8681	9.6850	7.6401	6.2682
	ω_3	46.4626	33.8121	21.7747	15.4924	11.9126	9.6449
	ω_4	82.5120	51.3783	30.5045	21.1554	16.0997	12.9690
	ω_5	128.7487	69.1418	39.0514	26.7262	20.2363	16.2615

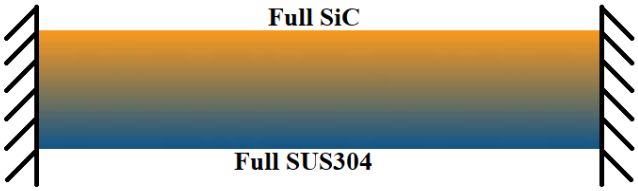

Fig. 4. Functionally graded C-C nanobeam

Table 3. Variation of first five frequencies (MHz) of FG nanobeam with k and e_0a/L (C-C)

k	**ω (MHz)**	**e_0a/L**					
		0	**0.1**	**0.2**	**0.3**	**0.4**	**0.5**
0	ω_1	23.7062	22.3654	19.3760	16.2643	13.6693	11.6421
	ω_2	65.3103	53.9796	38.5572	28.5806	22.3751	18.2819
	ω_3	127.9220	90.6560	57.6512	41.0566	31.6753	25.7224
	ω_4	211.2074	128.1562	75.6097	52.4448	39.9337	32.1811
	ω_5	315.0270	165.2416	93.2586	64.0399	48.6300	39.1599
0.2	ω_1	20.0006	18.8694	16.3471	13.7218	11.5325	9.8221
	ω_2	55.1000	45.5403	32.5288	24.1120	18.8767	15.4234
	ω_3	107.9189	76.4787	48.6349	34.6354	26.7212	21.6993
	ω_4	178.1710	108.1072	63.7804	44.2395	33.6858	27.1461
	ω_5	265.7327	139.3795	78.6615	54.0159	41.0180	33.0302
2	ω_1	13.8432	13.0603	11.3147	9.4976	7.9823	6.7985
	ω_2	38.1389	31.5225	22.5165	16.6905	13.0666	10.6763
	ω_3	74.7053	52.9434	33.6689	23.9776	18.4989	15.0223
	ω_4	123.3507	74.8490	44.1601	30.6307	23.3236	18.7956
	ω_5	183.9983	96.5172	54.4729	37.4063	28.4054	22.8738
5	ω_1	12.4760	11.7704	10.1972	8.5597	7.1940	6.1271
	ω_2	34.3727	28.4098	20.2932	15.0425	11.7765	9.6222
	ω_3	67.3299	47.7170	30.3455	21.6109	16.6729	13.5395
	ω_4	111.1767	67.4631	39.8028	27.6084	21.0223	16.9411
	ω_5	165.8462	86.9977	49.1007	33.7173	25.6041	20.6181
10	ω_1	11.7167	11.0541	9.5766	8.0387	6.7562	5.7542
	ω_2	32.2807	26.6807	19.0580	14.1269	11.0597	9.0365
	ω_3	63.2313	44.8121	28.4980	20.2951	15.6578	12.7152
	ω_4	104.4073	63.3549	37.3788	25.9271	19.7421	15.9094
	ω_5	155.7450	81.6980	46.1094	31.6632	24.0442	19.3619

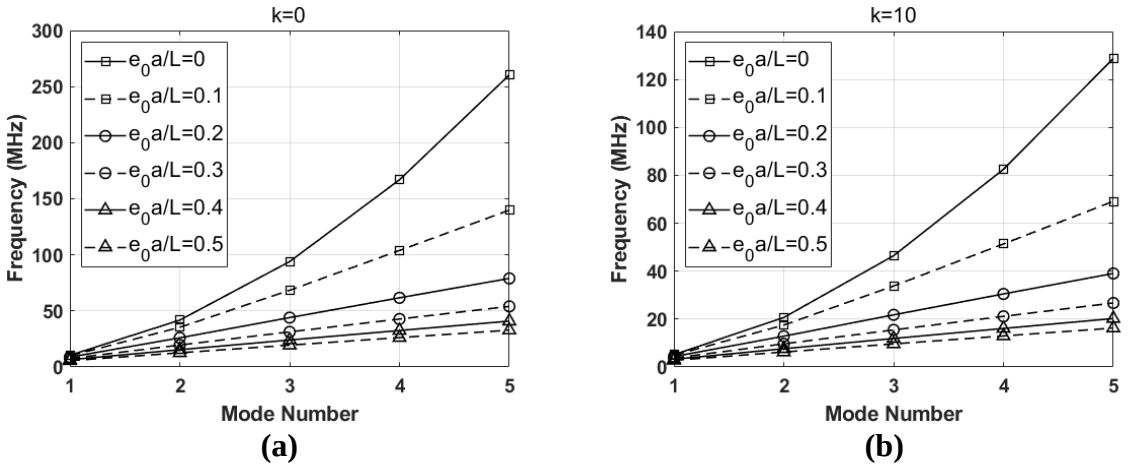

Fig. 5. The variation of the frequencies with mode numbers for different e_0a/L (S-S) (a) $k=0$ (b) $k=10$

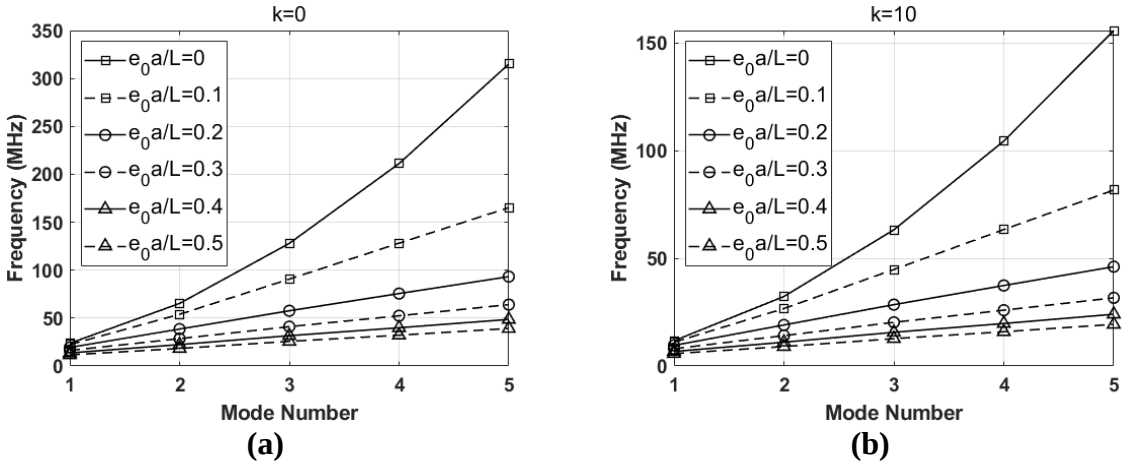

Fig. 6. The variation of the frequencies with mode numbers for different e_0a/L (C-C) (a) $k=0$ (b) $k=10$

The effects of mode number on the frequency are respectively shown in Fig. 5 and Fig. 6. The frequency values of FG nanobeam increase as the mode number increase.

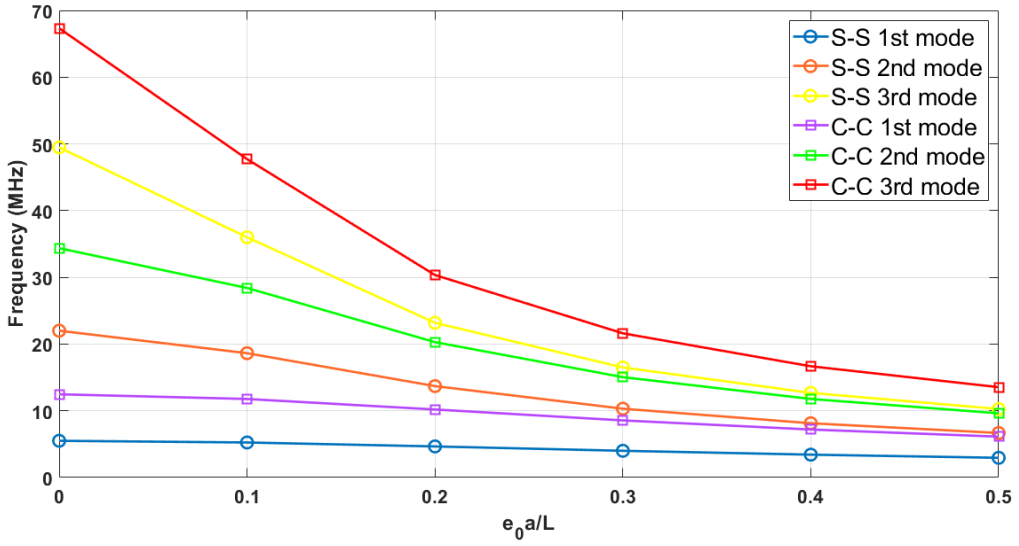

Fig. 7. The variation of the frequencies with e_0a/L ($k=5$)

The effects of e_0a/L (small-scale parameters) on the frequency are depicted in Fig. 7. The frequency values of FG nanobeam decrease as e_0a/L increases.

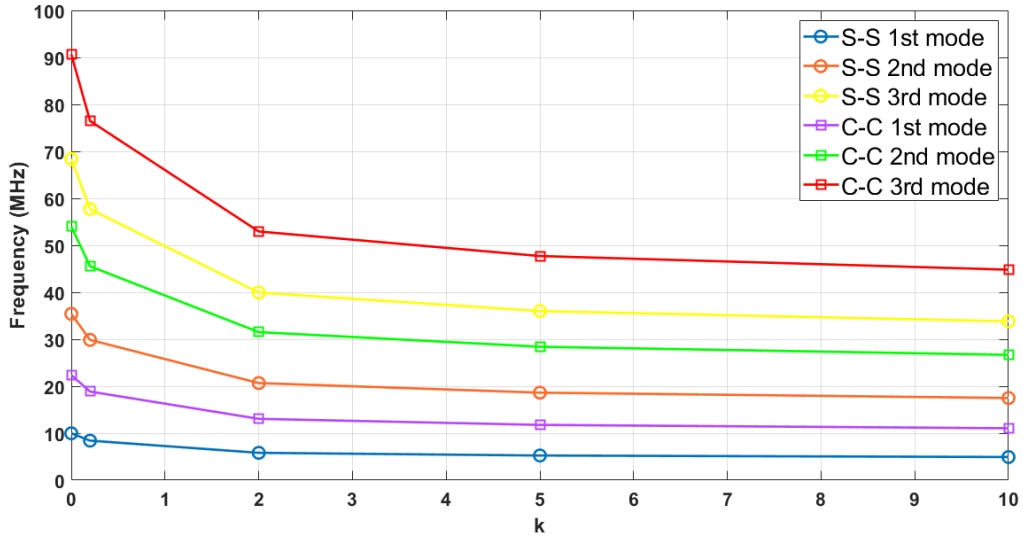

Fig. 8. The variation of the frequencies with k ($e_0a/L=0.1$)

The effects of k (power law exponent) on the frequency are depicted in Fig. 8. The frequency values of FG nanobeam decrease as k increases. Also it is clearly observed from the tables and figures that the frequency values of C-C boundary condition higher than the frequency values of S-S boundary condition.

6. Conclusions

Due to the small-scale effect, the properties and behaviours of nano structures are different from macro structures. In this paper, free vibration analysis of FG nanobeam composed of SiC and SUS304 is investigated based on the nonlocal elasticity theory and Euler-Bernoulli beam theory. Finite element method is a powerful numerical method. A nonlocal finite element formulation is developed for free vibration analysis of FG nanobeams, in this study. Solutions are obtained for S-S and C-C FG nanobeams. According to the obtained results

- By increasing e_0a/L, the frequency values decrease.
- Frequencies decrease with increasing k value.
- The frequency values of S-S smaller than the frequency values of C-C.
- The frequency values increase as the mode number increase.
- As the k increases, the properties of the FG nanobeam transform from ceramic to metal.

References

[1] Akgöz, B. and Civalek, Ö., Free vibration analysis of axially functionally graded tapered Bernoulli–Euler microbeams based on the modified couple stress theory. *Composite Structures*, 98, 314-322, 2013.

[2] Ebrahimi, F., Ghadiri, M., Salari, E., Hoseini, S.A.H. and Shaghaghi, G.R., Application of the differential transformation method for nonlocal vibration analysis of functionally graded nanobeams. *Journal of Mechanical Science and Technology*, 29(3), 1207-1215, 2015.

[3] Yayli, M.Ö. Torsional vibrations of restrained nanotubes using modified couple stress theory. *Microsystem Technologies*, 1-11, 2018.

[4] Ansari, R., Gholami, R., and Sahmani, S., Free vibration analysis of size-dependent functionally graded microbeams based on the strain gradient Timoshenko beam theory. *Composite Structures*, *94*(1), 221-228, 2011.

[5] Akgöz, B., and Civalek, Ö., Effects of thermal and shear deformation on vibration response of functionally graded thick composite microbeams. *Composites Part B: Engineering*, *129*, 77-87, 2017.

[6] Eringen, A.C., On differential equations of nonlocal elasticity and solutions of screw dislocation and surface waves. Journal of applied physics, 54(9), 4703-4710, 1983.

[7] Naghinejad, M. and Ovesy, H.R., Free vibration characteristics of nanoscaled beams based on nonlocal integral elasticity theory. *Journal of Vibration and Control*, 24(17), 3974-3988, 2018.

[8] Yaylı, M.Ö., Buckling Analysis of a Rotationally Restrained Single Walled Carbon Nanotube Embedded In An Elastic Medium Using Nonlocal Elasticity. *International Journal Of Engineering & Applied Sciences*, 8(2), 40-50, 2016.

[9] Eltaher, M.A., Emam, S.A. and Mahmoud, F.F., Static and stability analysis of nonlocal functionally graded nanobeams. *Composite Structures*, 96, 82-88, 2013.

[10] Thai, H.T., A nonlocal beam theory for bending, buckling, and vibration of nanobeams. *International Journal of Engineering Science*, 52, 56-64, 2012.

[11] Tounsi, A., Benguediab, S., Adda, B., Semmah, A. and Zidour, M., Nonlocal effects on thermal buckling properties of double-walled carbon nanotubes. *Advances in nano research*, 1(1), 1-11, 2013.

[12] Thai, S., Thai, H.T., Vo, T.P. and Patel, V.I., A simple shear deformation theory for nonlocal beams. *Composite Structures*, 183, 262-270, 2018.

[13] Ebrahimi, F. and Salari, E., Thermo-mechanical vibration analysis of nonlocal temperature-dependent FG nanobeams with various boundary conditions. *Composites Part B: Engineering*, 78, 272-290, 2015.

[14] Yayli, M.Ö., Buckling analysis of a cantilever single-walled carbon nanotube embedded in an elastic medium with an attached spring. *Micro & Nano Letters*, 12(4), 255-259, 2017.

[15] Yayli, M.Ö., On the axial vibration of carbon nanotubes with different boundary conditions. *Micro & Nano Letters*, 9(11), 807-811, 2014.

[16] Civalek, Ö., and Demir, C, Buckling and bending analyses of cantilever carbon nanotubes using the euler-bernoulli beam theory based on non-local continuum model. *Asian Journal of Civil Engineering*, 12(5), 651-661, 2011.

[17] Demir, Ç., and Civalek, Ö., A new nonlocal FEM via Hermitian cubic shape functions for thermal vibration of nano beams surrounded by an elastic matrix. *Composite Structures*, 168, 872-884, 2017.

[18] Naghinejad, M., and Ovesy, H.R., Viscoelastic free vibration behavior of nano-scaled beams via finite element nonlocal integral elasticity approach. *Journal of Vibration and Control*, 25(2), 445-459, 2019.

[19] Yayli, M.Ö., Effects of rotational restraints on the thermal buckling of carbon nanotube. *Micro & Nano Letters*, 14(2), 158-162, 2019.

[20] Mercan, K., Numanoglu, H.M., Akgöz, B., Demir, C. and Civalek, Ö., Higher-order continuum theories for buckling response of silicon carbide nanowires (SiCNWs) on elastic matrix. *Archive of Applied Mechanics*, 87(11), 1797-1814, 2017.

[21] Wang, C.M., Zhang, Y. Y., Ramesh, S.S. and Kitipornchai, S., Buckling analysis of micro-and nano-rods/tubes based on nonlocal Timoshenko beam theory. *Journal of Physics D: Applied Physics*, 39(17), 3904, 2006.

[22] Civalek, Ö. and Demir, Ç., Bending analysis of microtubules using nonlocal Euler–Bernoulli beam theory. *Applied Mathematical Modelling*, 35(5), 2053-2067, 2011.

[23] Kadıoğlu, H.G. and Yaylı, M.Ö., Buckling Analysis of Non-Local Timoshenko Beams by Using Fourier Series. *International Journal Of Engineering & Applied Sciences*, 9(4), 89-99, 2017.

[24] Zargaripoor, A., Daneshmehr, A., Isaac Hosseini, I., and Rajabpoor, A., Free vibration analysis of nanoplates made of functionally graded materials based on nonlocal elasticity theory using finite element method. *Journal of Computational Applied Mechanics*, 49(1), 86-101, 2018.

[25] Reddy, J.N., *Energy Principles and Variational Methods in Applied Mechanics*, John Wiley & Sons; 2nd edition, 2002.

[26] Talha, M. and Singh, B.N., Static response and free vibration analysis of FGM plates using higher order shear deformation theory. *Applied Mathematical Modelling*, 34(12), 3991-4011, 2010.

International Journal of Engineering & Applied Sciences (IJEAS)
Vol.11, Issue 2 (2019) 401-413
http://dx.doi.org/10.24107/ijeas.571192
Int J Eng Appl Sci 11(2) (2019) 401-413

Modal Analysis of Lenses Used in Automotive Lighting Industry and Obtaining MAC Matrix

Erhan Ay [a], Barış Ediz [b], Birhat Sönmezay [c] Sevda Telli Çetin [d]*

[a,b,c] R&D Department/Magneti Marelli Mako Elektrik Sanayi ve Ticaret A.Ş., Turkey
[d] Mechanical Engineering Department/Uludağ University, Turkey

E-mail address: erhan.ay@magnetimarelli.com [a*], baris.ediz@magnetimarelli.com [b], birhat.sonmezay@magnetimarelli.com [c], sevda@uludag.edu.tr [d]

ORCID numbers of authors:
0000-0001-9621-6030[a], 0000-0002-2704-7090[b], 0000-0002-8432-6192[c], 0000-0002-3281-9112[d]

Received date: 28.05.2019
Accepted date: 01.07.2019

Abstract

In this study, 4 different pieces of automotive rear lamp lenses which are made of Polymethylmethacrylate (PMMA) and have different geometries have been inspected. Free-free natural frequencies and mode shapes of lenses have been estimated by the help of ANSYS WB® Finite Element Analysis (FEA) software. Meanwhile, by the help of Experimental Modal Analysis (EMA) methods; natural frequencies, damping ratios and mode shapes of the lenses have been determined. Finally, mode shapes calculated by FE and measured by EMA were compared and Modal Assurance Criteria matrix (MAC) was determined. After experimental modal tests, FRF's were calculated by DEWESoft® X3 software then natural frequencies, damping ratios and mode shapes were calculated by the use of ME'scope® VESVT-570 Visual Modal software. In addition, MAC was calculated by the help of MEScope® software. The main reason for the use of such experimental methods was to understand if the assumptions made before theoretical analysis were satisfied in reality or not.

Keywords: Auotomotive Lighting, Polymethylmethacrylate, Finite Element Modal Analysis, Experimental Modal Analysis, Modal Assurance Criteria (MAC)

1. Introduction

The reaction of the structures used in engineering under the influence of static and dynamic forces is very important in the design phase of these structures. In order to investigate the reactions of the structures under the influence of dynamic forces, the free vibration characteristics must be determined in the first stage. Free vibration characteristics are the mode shapes of the structure, damping ratio and vibration frequencies. The comparison of the frequencies of the forces coming to the structure and the free vibration frequencies are important for the resonance event. In addition, it is very important to determine how the structure behaves under the influence of these forces in the investigation of the response of structures to dynamic forces.

The machines manufactured today are exposed to very high vibration forces due to their high speed and elastic structure. The frequencies of these forces are especially worth knowing about the resonance vibrations. Because, if the frequency of one or more of the driving forces coincides with the natural frequencies of the system, resonance vibrations with a destructive effect occur. Therefore, vibration analysis should be done at the design phase in order to avoid resonance vibrations and unwanted dynamic conditions. A number of simple studies that will be done during the design phase can prevent the future large vibration problems [1].

Altunel (2009) in his study, structural finite element model updating of a utility helicopter fuselage was performed as a case study. Initially, experimental modal analyses were performed using modal shakers. Modal analysis of test results was carried out using LMS Test.lab® software. At the same time, finite element analysis of the helicopter fuselage was performed by MSC.Patran & Nastran software. Initial updating was processed first for the whole helicopter fuselage then, tail of the helicopter was tried to be updated.

Furthermore, a new method was proposed for the optimum node removal location for getting better Modal Assurance Criterion (MAC) matrix. This routine was tried on the helicopter case study and it showed better performance than the Coordinate Modal Assurance Criterion (coMAC) that is often used in such analyses [2].

Gündoğan (2012) in her study, system identification of a model steel bridge has been performed and calibrated finite element model of the bridge is obtained. Although there are many different system identification types, in this study only NExT-ERA and ERA methods are used. Methods are programmed using Matlab. As a result of this study, modal parameters (mode shapes, natural frequencies, and damping ratios) of the structure has been estimated. On the other hand, modal assurance criteria (MAC) is calculated to mode shapes between NExT-ERA, ERA results and SAP2000 analysis results. It has been shown that mode shapes are in good agreement with each other. Natural frequencies, obtained from NExT-ERA and ERA, are also in good agreement [3].

Ay (2019), in his study; first of all, finite element undamped modal analysis was performed on one of the automotive rear lamp lenses and were obtained natural frequencies and mode shapes. Then, Frequency Response Functions (FRF) of an automotive rear lamp lens, made of polycarbonate (PC) material, were obtained by using Impact Hammer Test Methods. At the same time; dynamic characteristics of the structure, natural frequencies, damping ratios and mode shapes were obtained. Damping ratios were calculated from the FRF's by using the Half Power Method. Finite Element Analysis (FEA) results and test results were compared and the best test method was determined [4].

Ay (2019), in his study, the weight of the modal accelerometer used in the Roving Hammer Impact Test Method was added in the finite element analysis (FEA) and the undamped modal analysis of the automotive rear lamp lenses were performed. Also, calculated new Elastic Modulus for Polymethyl-methacrylate (PMMA) material with using natural frequency formula and this value was used in the ANSYS WB® program and the undamped modal analysis was repeated. After that, frequency response functions (FRFs) of an automotive rear lamp lens were obtained by using Roving Hammer Impact Test Method. At the same time; dynamic characteristics of the structure, natural frequencies, damping ratios and mode shapes were obtained. Damping ratios were calculated from the FRF's by using the Half Power Method. Finally, experimental modal analysis (EMA) and FEA results were compared [5].

The main aim of this study comparison of FEA results with the results of the Roving Hammer test for automotive rear lamp lenses made of PMMA material. EMA measurements were performed on the models. In order to make a comparison of experimental and analysis results, the analyses of the measured models with finite element method were also performed. In the EMA measurements, impact hammer and modal accelerometers were used. With the impact hammer at the points determined on the structures, the drive operation was carried out and the force applied to the structure with the force gauge at the end of the impact hammer was measured. Due to the applied force, the vibration in the structure was measured by the accelerometers placed at the determined points. The measured signals were processed in the DEWESoft® Sirius HD 16x STGS model data collection system to obtain FRF. FRF's were pre-controlled and natural frequencies were determined and the damping ratios corresponding to these natural frequencies were calculated by using the half power method.

Natural frequencies and mode shapes obtained by experiments and analysis were compared and Modal Assurance Criteria (MAC) was obtained. Then, the results obtained during the experiments and the results obtained from the comparison of experimental and theoretical results are presented.

2. Material and Method

2.1 Modal assurance criteria (MAC)

The MAC is used to determine the similarity of two mode shapes:

- If the mode shapes are identical (i.e., all points move the same) the MAC will have a value of one or 100%.
- If the mode shapes are very different, the MAC value will be close to zero.

If a mode shape was compared to itself, the MAC value should be one or 100%.

For modes with different shapes, the MAC is less than 1. Shapes that are very different will have a value close to zero. Mode shapes that are used in the comparison can originate from a Finite Element Analysis (FEA) or from an Experimental Modal Analysis (EMA). In a typical MAC analysis, one might make a 'MAC Matrix'. A 'MAC Matrix' is a series of bar graphs of MAC values, that each range from 0 to 100% as shown in Fig. 1.

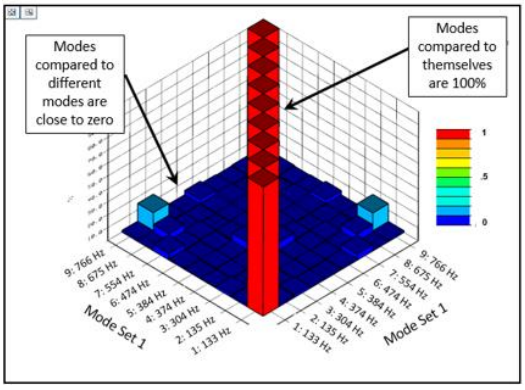

Fig. 1. MAC matrix comparing a set of 9 modes

In Fig. 1, the first mode shape at 133 Hz is identical to itself, hence a single red bar of a value of 1. Along the diagonal, every mode is identical to itself, 1 to 1 (133 Hz), 2 to 2 (135 Hz), 3 to 3 (304 Hz), etc.

Off of the diagonal, the MAC values are very low. Ideally, each mode should be uniquely observed and have a different shape than the other modes. This is the case for this mode set. The highest off diagonal mode pair is mode 2 compared to mode 9 (and vice versa 9 to 2) with a MAC value of 20%. All the other off-diagonal mode pairs are below 20% [6].

2.2 Modal assurance criterion equation

The MAC value between two modes is essentially the normalized dot product of the complex modal vector at each common nodes (i.e., points), as shown in Eq. (1). It can also be thought of as the square of correlation between two modal vectors Φr and Φs.

$$MAC\ (\{\Phi_r\},\{\Phi_s\}) = \frac{|\{\Phi\}_r^{*t}\ \{\Phi\}_s|^2}{(|\{\Phi\}_r^{*t}\ \{\Phi\}_r|)\ (|\{\Phi\}_s^{*t}\ \{\Phi\}_s|)} \quad (1)$$

where * and t represents the complex conjugate and transpose of the vector respectively. MAC value can have values only between 0 and 1. The value of 0 means that two vectors are orthogonal and there is no correlation between them. If the MAC value is 1, it means that vectors are fully correlated and equal to each other. The value below 0.3 are poorly correlated whereas above 0.8 are well correlated. Between these values, model can be updated to get MAC values above 0.8 [2].

A MAC analysis can be used in several different ways [7]:

- FEA - Test comparison: A MAC can be used to compare modes from an experimental modal analysis test to a FEA and an object. It will indicate if the same mode shapes are found in both the test and FEA analysis.
- FEA - FEA comparison: Several assumptions can be made in the creation of a FEA analysis: Young's Modulus, boundary conditions, and mass density values to name a few. A MAC analysis can determine the degree to which these assumptions affect the resulting mode shapes.
- Test - Test comparison: A MAC analysis can flag potential issues with the modal analysis results. Usually MAC will identify modes and areas that could benefit from acquiring more data points on the structure.

2.3 FEA of automotive rear lamp lenses

FEA was performed on automotive rear lamp lenses with 4 different geometries under free-free boundary conditions. For all lenses the first 3 flexible body mode shapes were investigated. In Fig. 2, Fig. 3 and Fig. 4, first, second and third flexible body mode shape are illustrated for the first sample respectively.

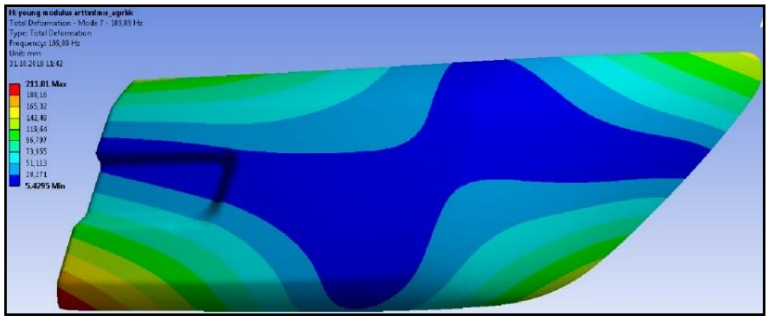

Fig. 2. First mode shape (109.89 Hz) for sample 1

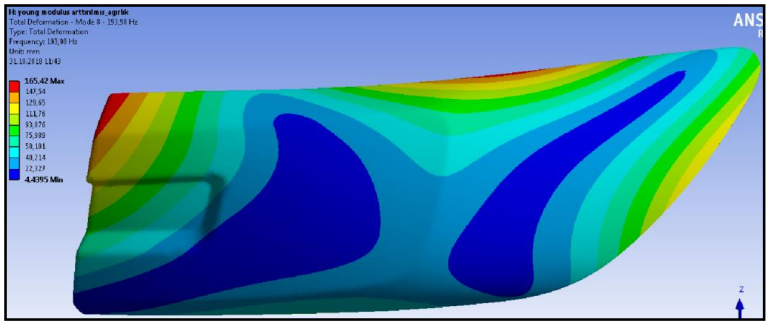

Fig. 3. Second mode shape (193.98 Hz) for sample 1

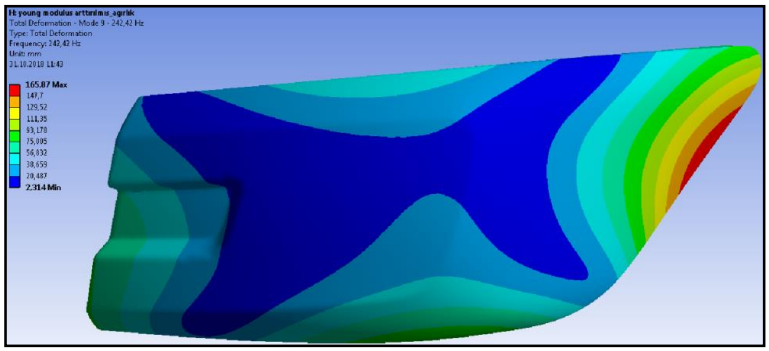

Fig. 4. Third mode shape (242.42 Hz) for sample 1

In Fig. 5, Fig. 6 and Fig. 7, first, second and third flexible body mode shape are illustrated for the second sample respectively.

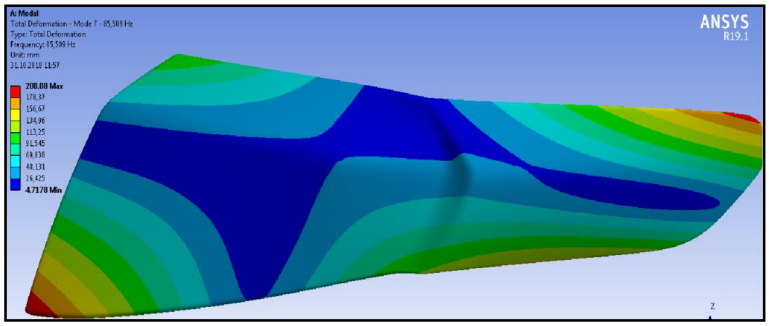

Fig. 5. First mode shape (85.509 Hz) for sample 2

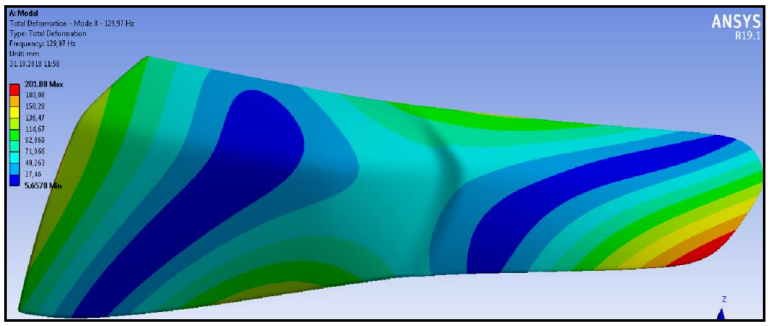

Fig. 6. Second mode shape (129.97 Hz) for sample 2

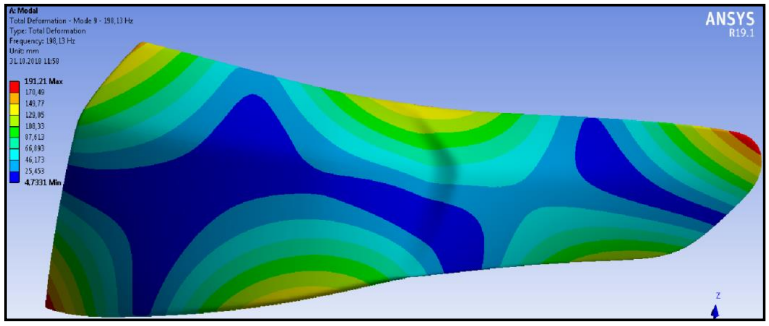

Fig. 7. Third mode shape (198.13 Hz) for sample 2

In Fig. 8, Fig. 9 and Fig. 10, first, second and third flexible body mode shape are illustrated for the third sample respectively.

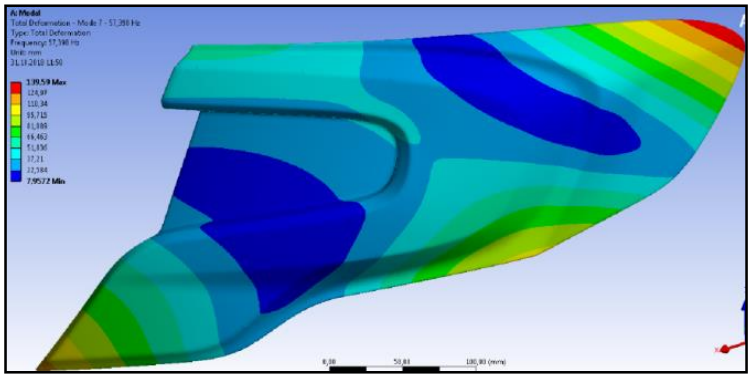

Fig. 8. First mode shape (57.398 Hz) for sample 3

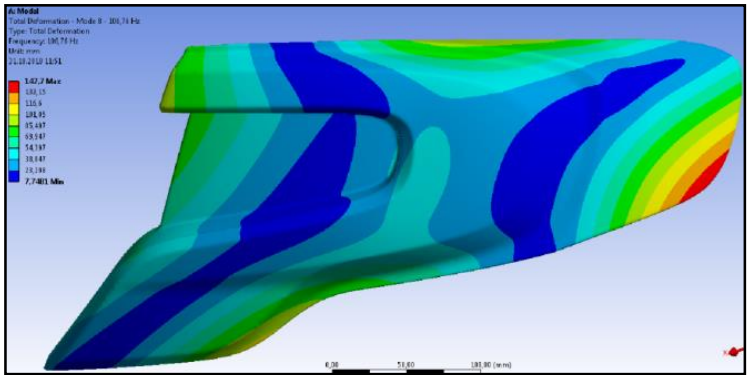

Fig. 9. Second mode shape (106.76 Hz) for sample 3

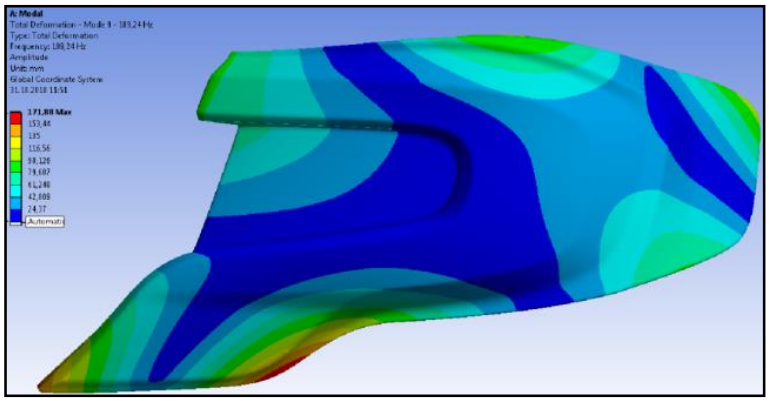

Fig. 10. Third mode shape (189.24 Hz) for sample 3

In Fig. 11, Fig. 12 and Fig. 13, first, second and third flexible body mode shape are illustrated for the fourth sample respectively.

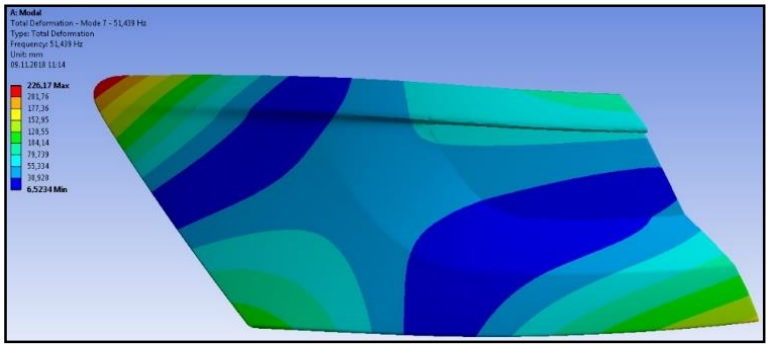

Fig. 11. First mode shape (51.489 Hz) for sample 4

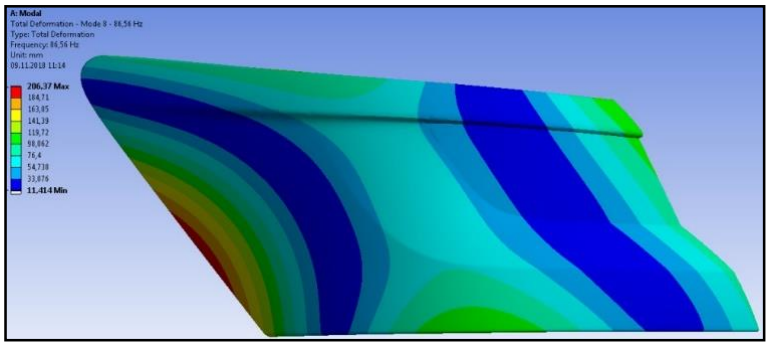

Fig. 12. Second mode shape (86.56 Hz) for sample 4

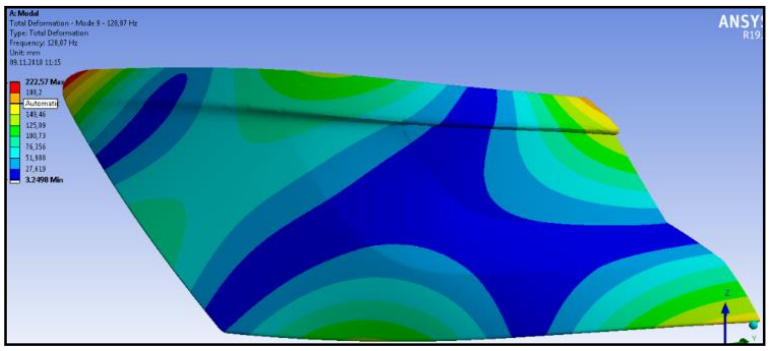

Fig. 13. Third mode shape (128.87 Hz) for sample 4

2.4 EMA of automotive rear lamp lenses

After FEA, EMA was performed on automotive rear lamp lenses with 4 different geometries. The lenses marked on the response and excitation points and was used impact hammer for test. Furthermore, the lenses were suspended from a single point to the testing apparatus using a single elastic rope to capture the condition closest to the free-free boundary conditions. For all lenses the first 3 flexible body mode shapes were investigated and the EMA natural frequency results were compared with the FEA natural frequency results. In Table 1, EMA natural frequency and FEA natural frequency results are illustrated for the first sample.

Table 1. FEA and EMA natural frequency results for sample 1

	FEA	EMA	(%)
1.Mod	109.89	110.871	0.884
2.Mod	193.98	201.230	3.602
3.Mod	242.42	393.477	38.390

In Table 2, EMA natural frequency and FEA natural frequency results are illustrated for the second sample.

Table 2. FEA and EMA natural frequency results for sample 2

	FEA	EMA	(%)
1.Mod	85.509	79.780	6.699
2.Mod	129.97	129.474	0.381
3.Mod	198.13	189.871	4.168

In Table 3, EMA natural frequency and FEA natural frequency results are illustrated for the third sample.

Table 3. FEA and EMA natural frequency results for sample 3

	FEA	EMA	(%)
1.Mod	57.398	56.682	1.247
2.Mod	106.76	102.437	4.049
3.Mod	189.24	189.595	0.187

In Table 4, EMA natural frequency and FEA natural frequency results are illustrated for the fourth sample.

Table 4 FEA and EMA natural frequency results for sample 4

	FEA	EMA	(%)
1.Mod	51.489	53.884	4.444
2.Mod	86.56	88.138	1.790
3.Mod	128.87	135.835	5.127

2.5 MAC calculation with using MEScope® software

MEScope® software is used to calculate the MAC. Mesh structure was imported to MEScope® software which including the points where acceleration measurements were made in EMA and FRFs measured at these points were taken. The FRFs were matched with these points. The curve is obtained for each FRF and the mode shapes are acquired.

Then the mesh structure and mode shapes used in the FEA model were imported into this software. These points are matched with the mode shapes. As a result of both EMA and FEA obtained mode shapes are examined.

Then, the points in the finite element mesh structure and the closest points in the mesh structure used in the EMA were matched.

After matching, mode shapes obtained by EMA and mode shapes obtained by FEA were compared using this program and MAC was calculated.

Thus, a validation was made between the FEA and the EMA.

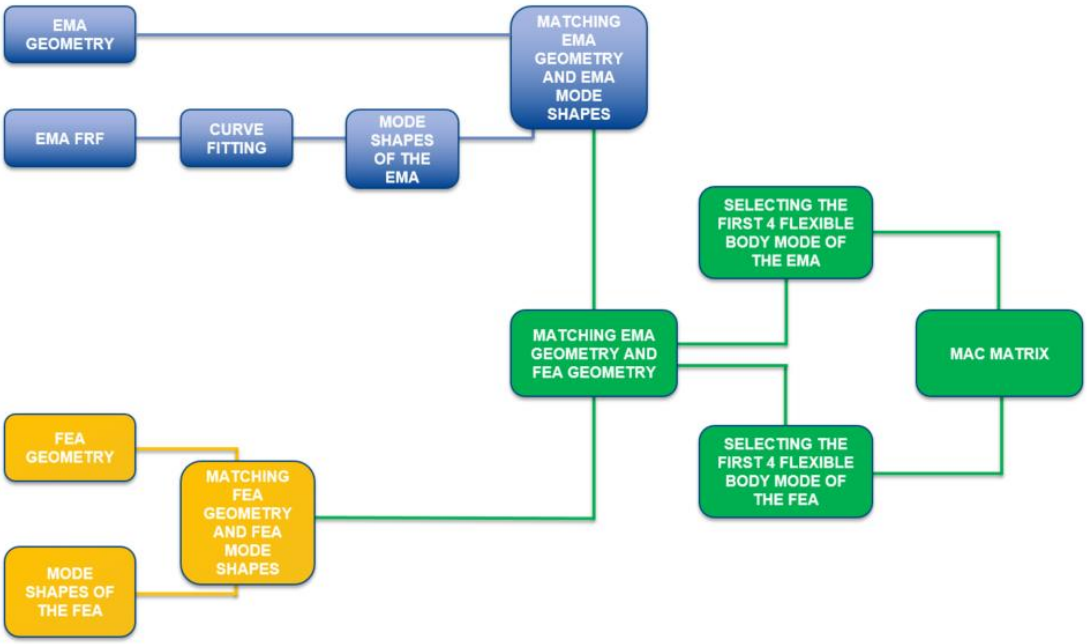

Fig. 14 MEScope® flow chart

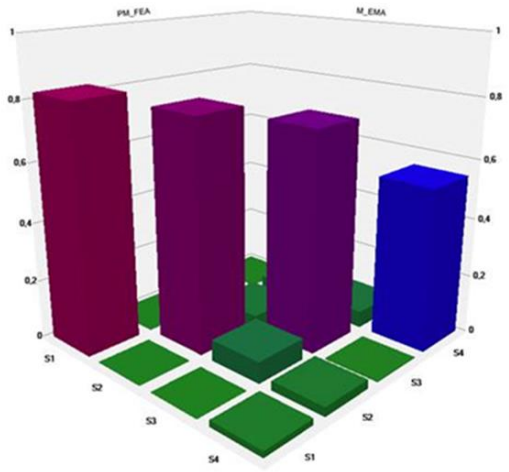

Fig. 15 MAC matrix for sample 1

					Shape 1	Shape 2	Shape 3	Shape 4
	Label	PM_FEA						
	M_EMA	Frequency(or Time)			112	201	386	508
			Damping		0	0	0	0
				Damping (%)	0	0	0	0
Shape 1	Global-Poly	114	3,13	2,74	0,822	0,00164	0,0481	0,00258
Shape 2	Global-Poly	205	6,9	3,36	0,00142	0,777	0,0456	0,0521
Shape 3	Global-Poly	407	9,59	2,36	4,87E-05	0,073	0,736	0,0567
Shape 4	Global-Poly	505	13,8	2,73	0,0212	0,0318	0,00295	0,548

Fig. 16 MAC table for sample 1

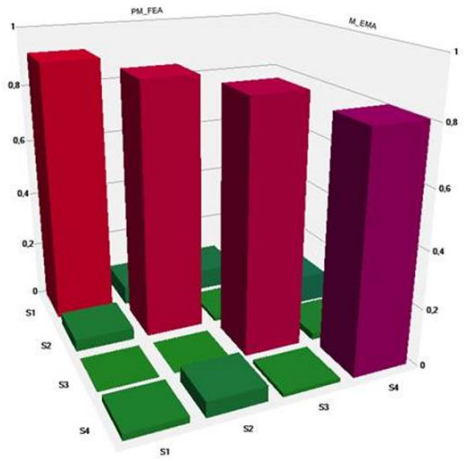

Fig. 17 MAC matrix for sample 2

					Shape 1	Shape 2	Shape 3	Shape 4
	Label	PM_FEA						
	M_EMA	Frequency(or Time)			85,5	130	198	264
			Damping		0	0	0	0
				Damping (%)	0	0	0	0
Shape 1	Global-Poly	81,1	3,53	4,35	0,916	0,0673	0,0747	0,00618
Shape 2	Global-Poly	128	4,31	3,36	0,0419	0,887	0,0144	0,102
Shape 3	Global-Poly	191	6,67	3,49	0,00237	0,00034	0,866	0,0246
Shape 4	Global-Poly	258	7,57	2,93	0,0226	0,0546	0,0136	0,808

Fig. 18 MAC table for sample 2

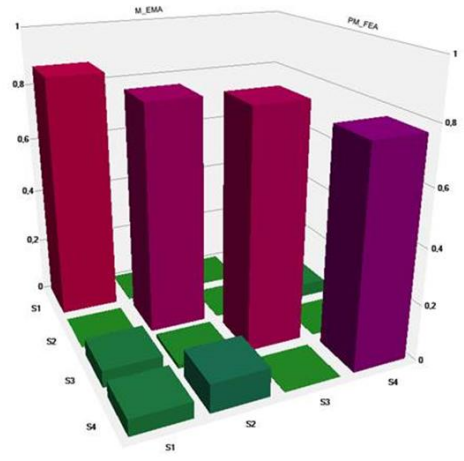

Fig. 19 MAC matrix for sample 3

					Shape 1	Shape 2	Shape 3	Shape 4
	Label	M_EMA			Global-Poly	Global-Poly	Global-Poly	Global-Poly
		Frequency(or Time)			56,3	102	190	221
	PM_FEA		Damping		1,73	3,09	5,05	6,21
				Damping (%)	3,08	3,03	2,66	2,82
Shape 1		57,4	0	0	0,867	0,00223	0,000353	0,00496
Shape 2		107	0	0	9,26E-05	0,816	0,00119	0,0494
Shape 3		189	0	0	0,0618	0,0157	0,839	0,000361
Shape 4		226	0	0	0,0584	0,101	0,00179	0,77

Fig. 20 MAC table for sample 3

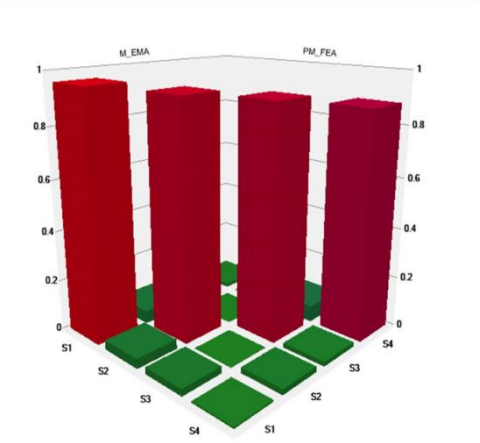

Fig. 21 MAC matrix for sample 4

					Shape 1	Shape 2	Shape 3	Shape 4
	Label	PM_FEA_Shape_Table						
		Frequency(or Time)			51,4	86,6	129	182
	PM_EMA_Shape_Table		Damping		0	0	0	0
				Damping (%)	0	0	0	0
Shape 1	Global-Poly	53,3	1,77	3,31	0,959	0,0386	0,0279	0,00669
Shape 2	Global-Poly	87,8	3,21	3,65	0,051	0,928	0,00161	0,0225
Shape 3	Global-Poly	133	3,79	2,85	0,0024	0,000795	0,908	0,0185
Shape 4	Global-Poly	184	7,7	4,19	0,0142	0,000481	0,0652	0,881

Fig. 22 MAC table for sample 4

3. Conclusions

In this study, experimental modal analysis test was performed on lenses produced from PMMA material used in automotive lighting industry. Test results and finite element modal analysis results were compared and MAC matrix was calculated using MEScope® software.

As a result;

- When looking at the similarity status of the first 4 modes for sample 1; 0.822, 0.777, 0.736, 0.548

- When looking at the similarity status of the first 4 modes for sample 2; 0.916, 0.887, 0.866, 0.808
- When looking at the similarity status of the first 4 modes for sample 3; 0.867, 0.816, 0.839, 0.77
- When looking at the similarity status of the first 4 modes for sample 4; 0.959, 0.928, 0.908, 0.881

it was found to be quite close to each other.

Notations

Φ_r EMA modal vector
Φ_s FEA modal vector

References

[1] Selman Tümer, T., Uçak kanadında titreşim analizi (Y. Lisans Tezi), CBÜ, Makine Mühendisliği Anabilim Dalı, Manisa, 2016.

[2] Altunel F., Modal updating of a helicopter structure using a newly developed correlation improvement technique (Y. Lisans Tezi), ODTÜ, Makine Mühendisliği Anabilim Dalı, Ankara, 2009.

[3] Gündoğan, M., Çelik model köprünün yapı sağlığının gözlenmesi (Y. Lisans Tezi), DEÜ, İnşaat Mühendisliği Anabilim Dalı, İzmir, 2012.

[4] Ay, E., Ediz, B., Çal, T., Telli Çetin, S., Modal analysis of automotive rear lamp lens produced from plastic material. *International Journal of Automotive Science and Technology, (under review)*, 2019.

[5] Ay, E., Ediz, B., Çal, T., Telli Çetin, S. ,Calculation of the modulus of elasticity with using natural frequency formula and updated finite element analysis of automotive rear lamp lens. *International Journal of Automotive Science and Technology,* 3 (2): 27-31, 2019.

[6]Anonymous, Modal assurance criterion (MAC). https://community.plm.automation.siemens.com/t5/Testing-Knowledge-Base/Modal-Assurance-Criterion-MAC/ta-p/368008, 2016.

[7] Pastor, M., Binda, M., Harčarik, T. 2012. Modal assurance criterion. *Science Direct.*